Investigator's Brochure

for

[^{18}F] fluoromisonidazole, 1H-1-(3-[^{18}F]-fluoro-2-hydroxy-propyl)-2-nitro-imidazole, [^{18}F]FMISO

An Investigational Positron Emission Tomography (PET) radiopharmaceutical for injection and intended for use as an in vivo diagnostic for imaging hypoxia in tumors.

IND # put your IND# here

Put your Name and Address here

IB Edition Number: 7
IB Edition Date/Release Date: December 2, 2021

I. TABLE OF CONTENTS 2

TABLE OF TABLES

TABLE OF FIGURES

II. [^{18}F]FMISO PRODUCT AGENT DESCRIPTION

1. AGENT DESCRIPTION

Fluorine-18 labeled misonidazole, 1H-1-(3-[^{18}F]-fluoro-2-hydroxy-propyl)-2-nitro-imidazole, or [^{18}F]FMISO, is a radiolabeled imaging agent that has been used for investigating tumor hypoxia with positron emission tomography (PET). The University of Washington pioneered the development and biodistribution evaluation of [^{18}F]FMISO. An ideal hypoxia-imaging agent should distribute independently of blood flow, which is best achieved when the partition coefficient of the tracer is close to unity. Under these circumstances, imaging can be done at a time when the intracellular tracer distribution has equilibrated with the tracer in plasma near the cells. [^{18}F]FMISO is an azomycin-based hypoxic cell sensitizer that has a nearly ideal partition coefficient and, when reduced by hypoxia, binds covalently to cellular molecules at rates that are inversely proportional to intracellular oxygen concentration, rather than by any downstream biochemical interactions.[1]

2. CHEMICAL STRUCTURE

[^{18}F]FMISO has not been marketed in the United States and, to the best of our knowledge, there has been no marketing experience with this drug in other countries. The radiopharmaceutical product, [^{18}F]FMISO is the only active ingredient and it is dissolved in a solution of ≤10 mL of 95% isotonic saline 5% ethanol (v:v). The drug solution is stored in at room temperature in a gray butyl septum sealed, sterile, pyrogen-free glass vial with an expiration time of 12 hours. The injectable dose of [^{18}F]FMISO for most studies will be ≤ 10 mCi of radioactive ^{18}F at a specific activity of greater than 125 Ci/mmol at the time of injection. In the dose of [^{18}F]FMISO only a small fraction of the FMISO molecules are radioactive. The amount of injected drug is ≤ 15 µg (≤ 80 nmol per dose) of FMISO. [^{18}F]FMISO is administered to subjects by intravenous injection of ≤ 10 mL.

There is no evidence that nonradioactive and radioactive FMISO molecules display different biochemical behavior.

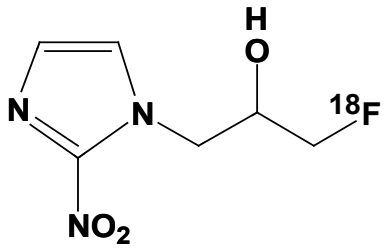

Figure 1. The chemical structure of [^{18}F]-fluoromisonidazole

1H-1-(3-[^{18}F]-fluoro-2-hydroxy-propyl)-2-nitro-imidazole

3. FINAL PRODUCT SPECIFICATIONS

The product components are listed in Table 1, the impurities in Table 2, and the final product specifications in Table 3.

Table 1. Final Product Components per single injected dose

COMPONENTS	Characterization	Amount in Injectate
[^{18}F]FMISO, 1H-1-(3-[^{18}F]-fluoro-2-hydroxy-propyl)-2-nitro-imidazole	Same as for [^{19}F]FMISO	≤ 10 mCi
[^{19}F]FMISO, 1H-1-(3-[^{19}F]-fluoro-2-hydroxy-propyl)-2-nitro-imidazole	NCS#292930	≤ 15 µg
Ethanol, absolute	USP	5% by volume
Saline for injection	USP	0.15 M

Table 2. Final Product Impurities per single injected dose

IMPURITIES	Acceptance Criteria	Highest Values in 9 Qualification Runs
Kryptofix® [2.2.2]	< 50 µg/mL	None detected
Acetonitrile	≤ 410 ppm	< 50 ppm
Acetone	≤ 5000 ppm	< 313 ppm
Other UV absorbing impurities	≤ 35 µg	4.9 µg (1 hr post synthesis)

Table 3. Final Product Specifications

TEST	SPECIFICATION
Chemical Purity (particulates)	Clear and Colorless
pH	4.5-8
Residual Kryptofix® [2.2.2]	< 50 µg/ mL Kryptofix®
Radiochemical Purity (HPLC)	≥ 95%
Chemical Purity (HPLC)	FMISO ≤ 15 µg/dose Other compounds ≤35µg/dose
Radiochemical Purity (TLC)	Rf >0.5 Purity ≥ 95%
Residual Solvent Levels	Acetone ≤ 5000 ppm Acetonitrile ≤410 ppm
Radionuclidic Purity	Measured half-life 100-120 minutes
Bacterial Endotoxin Levels	< 175 EU per dose
Sterility	Negative/no growth, must also pass filter integrity test
The drug solution is stored at room temperature in a septum sealed, sterile, pyrogen-free glass vial with an **expiration** time of **12 hours**	

The specifications that have been updated are for pH and acetonitrile. The purity specifications have been clarified to ≥ instead of > to avoid ambiguity. These changes are not considered major and will not increase risk to the patient. Justification for these changes is to align these specifications with similar FDA approved PET radiopharmaceuticals and the ICH guidelines. Many sites are now preparing FMISO with prefilled cassettes and automated synthesis instruments that were designed in compliance with these newer published limits.

1. Acetonitrile is listed in the Guidance for Industry, QC3 – Tables and List, Revision 2, February 2012 as a class 2 solvent with a concentration limit of 410 ppm. Acetone is a class 3 solvents and limited to 5000 ppm so no specification change is needed for them.

2. FDA approved labeling for two very similar radiopharmaceuticals, F-18 FDG and NaF F18, has both drugs specified at pH 4.5-8. To be consistent with these drugs, we have changed the F-18 FMISO specification to 4.5-8.1.

III. INTRODUCTION

[^{18}F]-fluoromisonidazole ([^{18}F]FMISO) is a radiolabeled imaging agent that has been used for investigating tumor hypoxia with positron emission tomography (PET). [^{18}F] decays by positron emission. FMISO binds covalently to cellular molecules at rates that are inversely proportional to intracellular oxygen concentration. In hypoxic cells, FMISO is trapped, which is the basis for the use of this tracer to measure hypoxia. Because tissue oxygenation may serve as a marker of perfusion, response to radiotherapy and chemotherapy, tumor grade, and prognosis, development of a PET imaging agent for tumor hypoxia is a potentially valuable avenue of investigation.

Positron emission tomography (PET) is a quantitative tomographic imaging technique, which produces cross-sectional images that are composites of volume elements (voxels). In PET images, the signal intensity in each voxel is dependent upon the concentration of the radionuclide within the target tissue (e.g., organ, tumor) volume. To obtain PET imaging data, the patient is placed in a circumferential detector array.

Patients undergo two separate imaging studies in a typical PET imaging procedure. One is a transmission scan via a germanium rod source or, in the case of PET-CT, by CT imaging of the body region(s) of interest. The second component of the study is the emission scan which can be a dynamic imaging acquisition over a specific area of interest, or multiple acquisitions over the whole body. The typical PET study takes 20 minutes to 2 hours to perform depending upon the nature of the acquisitions and the areas of the body that are imaged.

The [^{18}F]FMISO radiotracer (≤ 10 mCi) is administered by intravenous injection. Imaging can commence immediately upon injection for a fully quantitative study over one area of the body. More often only a static image is acquired for a 20-minute interval beginning between 100 and 150 minutes post injection.

IV. PHARMACOLOGY

1. PHYSICAL CHARACTERISTICS

Fluoromisonidazole is a small, water-soluble molecule with a molecular weight of 189.14 Daltons. It has an octanol:water partition coefficient of 0.41, so that it would be expected to reflect plasma flow as an inert, freely-diffusible tracer immediately after injection, but later images should reflect its tissue partition coefficient in normoxic tissues.

2. MECHANISM OF ACTION

[^{18}F]FMISO is an azomycin-based hypoxic cell sensitizer that has a nearly ideal partition coefficient and, when reduced by hypoxia, binds covalently to cellular molecules at rates that are inversely proportional to intracellular oxygen concentration, rather than by any downstream biochemical interactions[1]. The covalent binding of nitroimidazoles is due to bioreductive alkylation based on reduction of the molecule through a series of 1-electron steps in the absence of oxygen[2]. Products of the hydroxylamine, the 2-electron reduction product, bind stably in cells to macromolecules such as DNA, RNA, and proteins. In the presence of oxygen, a futile cycle results in which the first 1-electron reduction product, the nitro radical anion, is re-oxidized to the parent nitroimidazole, with simultaneous production of an oxygen radical anion. FMISO is not trapped in necrotic tissue because mitochondrial electron transport is absent. The normal route of elimination for FMISO is renal. A small fraction of [^{18}F]FMISO is glucuronidated and excreted through the kidneys as the conjugate.

V. TOXICOLOGY AND SAFETY

1. MECHANISM OF ACTION FOR TOXICITY

Therapeutic Implications of Hypoxia. Tumor physiology differs from that of normal tissue in several significant ways. Circumstances within tumor tissue can result in hypoxia when growth outpaces angiogenesis or when the oxygen demands of accelerated cellular proliferation exceed local oxygen concentrations. Because hypoxia increases tumor radioresistance, it is important to identify patients whose disease poses this risk for therapeutic failure, lest hypoxic cells survive radiotherapy while retaining their potential to proliferate[3,4]. The selectivity of nitroimidazoles for hypoxic conditions has been demonstrated in rat myocytes[5,6], the gerbil stroke model[7,8], pig livers[9,10], rat livers[11,12] and dog myocardium[13,14], as well as numerous cancer studies in cell cultures, animals and human trials[15,16].

The mechanism of action of FMISO is common to all nitroimidazoles and is based on the chemical reduction that takes place in hypoxic tissue, covalently binding the chemical to macromolecules in that tissue. The specificity of the reaction is enhanced by the fact that both the reduction and the binding occur within the same cell[17,18]. The reduction reaction, depicted in Figure 2, is reversible at the first step, depending upon the oxygenation status of the tissue, so that some FMISO eventually returns to the circulation and is excreted[19]. The reduction of the nitro group on the imidazole ring is accomplished by tissue nitroreductases that appear to be plentiful and therefore do not represent a rate-limiting factor[1]. The 1-electron reduction product (labeled as "II" in Figure 2) may be further reduced to "III" or it may competitively transfer its extra electron to O_2 and thus reform "I." This binding takes place at a rate that is inversely related to cellular oxygen concentration[6].

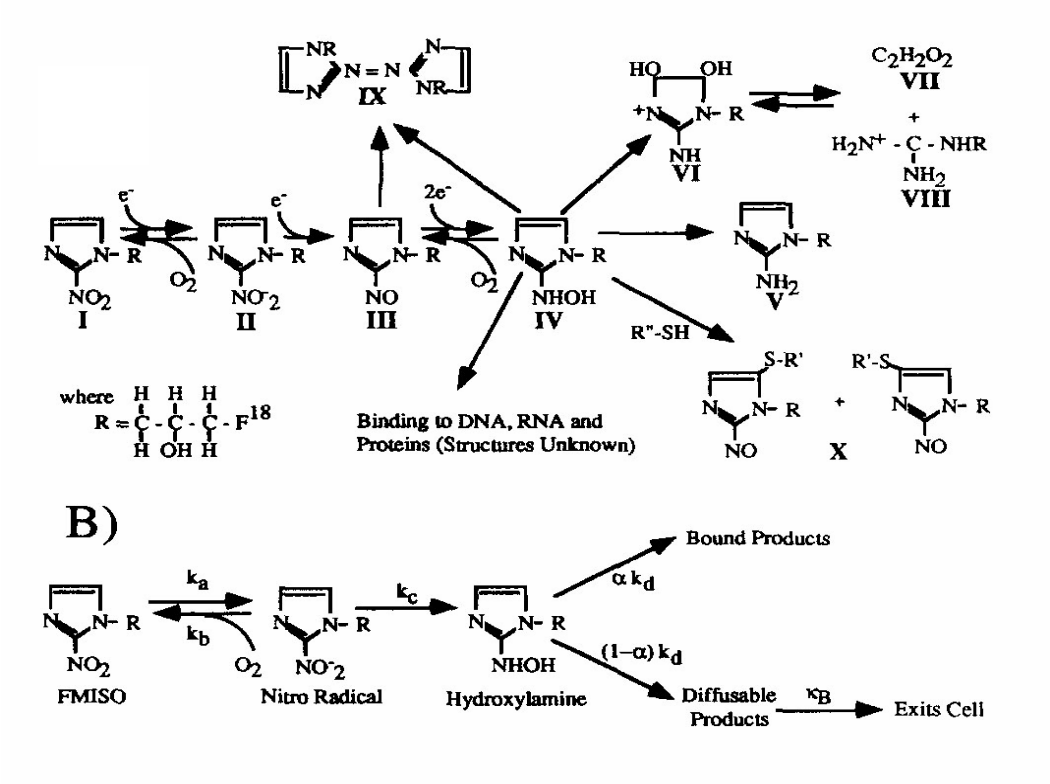

Figure 2. Metabolism of 2-nitroimidazoles.
See text (above figure) for further details

Nitroimidazoles bind to hypoxic tissue, serving as hypoxia markers. They potentiate the cytotoxic effects of some chemotherapeutic agents such as the nitrosoureas, melphelan and cyclophosphamide[20,21]. Identifying hypoxic tissue has therapeutic implications for multiple disease states including stroke, myocardial ischemia, and is of particular value in cancer radiotherapy, as hypoxic cancer tissue is relatively radioresistant[22]. These chemical properties suggested the possibility of clinically imaging hypoxic tissue in vivo. Misonidazole, or a related compound, could be labeled with a radioisotope, and could bind to oxygen-deprived cells covalently, providing a positive image of hypoxia via PET. Fluoromisonidazole (Figure 1) has several properties that make it a potentially useful imaging agent. In contrast to the prototype molecule, misonidazole, FMISO can be labeled at the end of the alkyl side chain with ^{18}F, a positron emitter with a 110 minute half-life[23,24]. Fluorine-carbon bonds are highly stable and so the radioactive ^{18}F would be expected to remain on the molecule of interest.

MISO and fluoromisonidazole (FMISO) are 2-nitroimidazoles with nearly identical octanol:water partition coefficients, making them sufficiently lipophilic that they readily diffuse across cell membranes and into tissues[25], yet maintain a volume of distribution essentially equal to total body water[26]. They are less than 5% protein bound, allowing efficient transport from blood into tissues[17]. The distribution kinetics of 2-nitroimidazoles fit a linear two-compartment open model, except that high plasma

concentrations after therapeutic level (gram) injections appear to saturate elimination processes in both mice and humans and proceed to non-linear kinetics.

Metabolism and Elimination. *In vitro,* MISO can be reduced using zinc, iron in HCl, xanthine oxidase and NADH[1]. In HeLa and CHO (hamster ovary) cells, reduction appears only under hypoxic conditions. Comparison with MISO indicates that the reduction reaction is similar, but slightly slower for FMISO[1]. FMISO achieves higher tumor:blood and tumor:muscle concentration ratios than MISO in murine tumors[27].

In vivo, under normal oxygen tension, MISO is metabolized primarily in the liver to its demethylated form but FMISO is not a substrate for this reaction. Additionally, ~7% (in humans) to ~14% (in mice) is conjugated to glucuronide, and small amounts (<5%) are converted to aminoimidazole. Substantial amounts of MISO are recoverable in feces. Fecal bacteria are able to reduce misonidazole only in the absence of oxygen. At treatment level dosing, the plasma half-lives of both FMISO and MISO range from 8 – 17.5 hours[28]. Parent molecule and glucuronide metabolites are primarily excreted in the urine[29,30,31].

FMISO Mouse Studies. Biodistribution studies in mice have used different transplanted tumors and compared [^{3}H]FMISO with the [^{18}F]FMISO. The only normal organs with significant uptake were those associated with nitroimidazole metabolism and excretion, i.e. liver and kidney. Mice bearing a variety of tumors of different sizes received a single injection of [^{3}H]FMISO and were sacrificed at 4 hr[32]. The results are shown in Table 4. For small KHT tumors, the tumor to blood ratios (T:B) of 2.3-2.9 were sufficiently high to allow tumor detection with imaging. Larger KHT tumors, with a reported hypoxic fraction >30%, had higher T:B ratios. RIF1 tumors in C3H mice have a hypoxic fraction of ~1.5% and had the lowest tumor:blood ratios: 1.7-1.9. This correlation between T:B ratios and hypoxic fraction was encouraging, but did not hold true across all tumor types. C3HBA mammary adenocarcinomas of the same size as the RIF1 and small KHT tumors, had hypoxic fractions of 3-12%, but had the highest T:B ratios, 4.0-4.7. Within tumor type, increasing hypoxia was associated with increased uptake of labeled FMISO, but comparisons across tumor types were more difficult, perhaps because of heterogeneity within the tumors.

Table 4. Biodistribution of [^{3}H]fluoromisonidazole in C3H mice[32]

Tumor	Drug dose	Tumor: Blood ratios	Tumor volumes. mm^{3*}	Estimated hypoxic fraction$^+$
KHT	5 mmol/kg	2.41	175 ± 16	7-12%
KHT	5 mmol/kg	2.29	110 ± 25	
KHT	20 mmol/kg	2.76	159 ± 39	
KHT	20 mmol/kg	2.86	123 ± 37	
KHT	5 mmol/kg	5.58	580 ± 26	>30%
KHT	5 mmol/kg	8.34	574 ± 66	
RIF1	5 mmol/kg	1.69	158 ± 23	~1.5%
RIF1	20 mmol/kg	1.76	159 ± 15	
RIF1	20 mmol/kg	1.86	136 ± 37	
C3HBA	5 mmol/kg	4.66	101 ± 13	3-12%
C3HBA	5 mmol/kg	3.96	137 ± 37	

* Tumor volumes are mean ± standard deviation for 5 tumors/group. Animals sacrificed at 4 hr.
+ Hypoxic fractions are taken from Moulder 1984 Vol10 P695-712[33] for tumors of comparable size.

In individual KHT tumors or RIF1 tumors, there was no correlation between regional flow and regional FMISO retention at 4 hr after tracer injection. The r^2-values for KHT and RIF1 tumors were 0.0 and 0.05, respectively. Regional blood flow did not correlate with FMISO retention in normal tissues that retained high levels of FMISO, specifically in liver (a principal site of nitroimidazole metabolism) and kidney (the main route of excretion) nor in tissues such as muscle and brain.

The mouse biodistribution studies described above provided useful information about relative tumor FMISO distribution at a single time post-injection and demonstrated T:B ratios adequate for PET imaging. Tumor bearing rats have also been imaged dynamically to provide biodistribution data for all tissues after sacrifice. The well-characterized 36B10 transplantable rat glioma was grown subcutaneously in Fischer rats[34] to obtain time-activity data for tumors and blood up to 2 hr after FMISO injection. These studies showed that tumors steadily accumulated [^{3}H]FMISO activity that exceeded levels in blood after ~20 min.

Dogs with spontaneous osteosarcomas, a tumor that is frequently radio-resistant, have also been imaged after injection of [^{18}F]FMISO. These images allowed the investigator to draw regions of interest around tumor and normal tissue in each imaging plane. Timed blood samples were also drawn and plasma was counted in a gamma well so that, after decay correction, imaging and blood data could be converted to units of µCi/g. Blood

time-activity curves for dogs were similar when presented in comparable units[32]. Time-activity curves for blood, muscle and for a region from a forelimb osteosarcoma in one dog are shown in Figure 3.

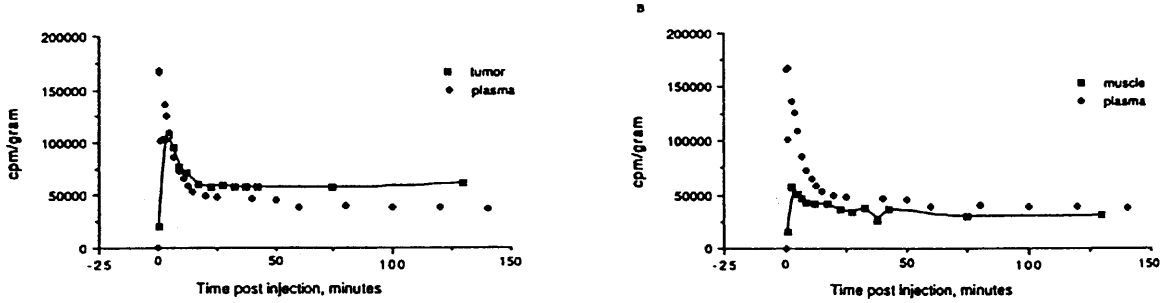

Figure 3. FMISO blood and tissue clearance curves in a dog with osteosarcoma

Muscle equilibrated with blood after 60 min, while the selected tumor region continued to accumulate FMISO above blood levels. The mean plasma half-time, calculated from five dogs, was 284±20 min for the slow component. The dog studies showed marked regional variation in FMISO uptake. These imaging studies with dogs confirmed the feasibility of imaging and suggested that multi-plane images in individual tumors would be necessary to assess regional variation in tumor hypoxia.

2. FMISO CELL TOXICITY STUDIES

Early studies evaluating the biological behavior of FMISO used several model systems with varying levels of complexity. The studies performed *in vitro* employed cells in monolayer cultures and multi-cellular spheroids. Multicellular spheroids are aggregates of cells that grow in culture and mimic small nodular tumors. Cell uptake and distribution studies in spheroids were done using [^{3}H]FMISO[35].

The *in vitro* studies of tumor cells and rodent fibroblasts measured the O_2-dependency of FMISO uptake and the time course of uptake at O_2 levels approaching anoxia. Uptake of FMISO by cells growing in monolayer cultures depended strongly on oxygen concentration, with maximum uptake under anoxic conditions and a decrease to 50% of maximum binding at levels between 700 to 2300 ppm in several different cell lines (Table 4a). The O_2-dependency of binding was a mirror image of the curve for sensitization to radiation by O_2, an advantageous characteristic for a hypoxia tracer intended to assess radiobiologically significant levels of hypoxia.

Table 5. Inhibition of [^{3}H]FMISO Binding by Oxygen *in vitro*[36]

Cell Line	O_2 concentration to inhibit binding by 50% (ppm)
RIF1	720
V79	1400
EMT6	1500
CaOs1	2300

Uptake of FMISO by multi-cellular spheroids provided visual and quantitative measures of hypoxia. Autoradiographs of 0.8 mm V79 spheroids after 4 hr incubation with [^{3}H]FMISO revealed heavily labeled cells in an intermediate zone between the well oxygenated periphery and the necrotic center. Uptake in anoxic spheroids matched that in anoxic monolayer cultures; oxygenated spheroids did not accumulate tracer, and hypoxic spheroids had intermediate uptake.

Whitmore et al. performed preliminary toxicity studies on MISO using Chinese hamster ovary cells[37]. Uncharacterized toxic products suspected of being either nitroso or hydroxylamine derivatives formed only under hypoxic conditions and were capable of sensitizing both hypoxic and aerobic cells to the damaging effects of radiation. These products have been further characterized by Flockhart and are differently distributed depending upon the species. In humans the demethylated molecule never exceeds 10% of the total MISO, and the amine never exceeds 2% in extracellular fluid[31]. The demethylation reaction is not possible with FMISO, which lacks a methoxy substituent.

3. ANIMAL TOXICITY STUDIES: MISO and FMISO

The literature provides a few animal studies of the toxicity of nitroimidazoles. The octanol/water partition coefficients for MISO and FMISO are 0.43 and 0.41, respectively; the LD50's in adult male Balb/C mice for MISO and FMISO are 1.8 mg/g (1.3-2.6) and 0.9 mg/g, respectively[38]. The serum half-lives of orally administered MISO and FMISO in mice were 2.3 hrs (range 1.87-2.92) and 2.0 hrs (range 1.79-2.24), respectively. A subsequent study of LD50's in 21 to 32 g, nine-month old, female C3H/HeJ mice gave toxicities of 0.62 to 0.64 mg/g for FMISO[39]. The long component of the plasma half-life of FMISO in humans is similar to MISO (8-17 hrs). FMISO is cleared primarily through the kidneys. Its volume of distribution is large, approximating that of total body water. Favorable tumor-to-normal tissue ratios for imaging are obtained at low doses of administered drug. These ratios were obtained in 15 kg dogs with a dose of 1 mg/kg.

After oral dosing that exceeds a schedule-dependent cumulative threshold, misonidazole induces a peripheral neuropathy in humans, although such dosing far exceeds the PET imaging dose requirements. Because FMISO will be administered intravenously, the neurotoxicity of intravenous administration was evaluated in rats using a battery of routine clinical, neurofunctional, biochemical, and histopathologic

screening methods[40]. Male Sprague-Dawley rats were administered intravenous doses of misonidazole at 0 (vehicle control), 100, 200, 300, or 400 mg/kg daily for 5 days per week for 2 weeks. Animals were evaluated for functional and pathological changes following termination of treatment and at the end of 4 weeks. During the dosing phase, hypoactivity, salivation, rhinorrhea, chromodacryorrhea, rough pelage and ataxia were observed at 400 mg/kg and body weight gain of the 300 and 400 mg/kg groups was significantly decreased relative to the vehicle controls (24% and 49% respectively) and related to reductions in food consumption of 8% and 23%. Although most 400 mg/kg animals appeared normal immediately after the dosing regimen, rotorod testing precipitated a number of clinical signs including: ataxia, impaired righting reflex, excessive rearing, tremors, vocalization, circling, head jerking, excessive sniffing and hyperactivity. All animals recovered and appeared normal through study termination. There were no treatment-related effects on motor activity, acoustic startle response, rotorod performance, forelimb group strength, toe and tail pinch reflexes, tibial nerve beta-glucuronidase activity or tail nerve conduction velocity. No microscopic changes were detected in peripheral nerves. Necrosis and gliosis were seen in the cerebellum and medulla of the 400 mg/kg animals after treatment and gliosis in these same brain regions was observed in the 300 and 400 mg/kg groups at a month after dosing. These results show that intravenous administration of misonidazole to rats causes dose-limiting central nervous system toxicity without effects on peripheral nervous tissue.

4. HUMAN TOXICITY STUDIES: MISO

Human studies of nitroimidazoles date back to the 1970's when several nitroimidazole derivatives were tested as oxygen mimetics in clinical research trials involving tumors that were presumed to be hypoxic. The goal was to sensitize them to cytotoxic levels of photon radiation so that they retained the beneficial 3-fold enhancement ratio characteristic of normoxic tissues[41,42,43]. Our knowledge of the toxic effects of 2-nitroimidazoles in humans is based principally on misonidazole, a close analog of fluoromisonidazole (Figure 1), and studies that used doses that were considered effective to enhance the cytotoxicity of radiotherapy. These human studies, no longer in progress, have been reviewed[44]. There have been no reported harmful effects until cumulative doses exceeded a few grams, which is approximately 5 to 6 orders of magnitude greater than the dosing required for PET imaging.

Gray reported preliminary human pharmacokinetic measurements using six healthy volunteers[45]. Subjects received single oral doses ranging from 1 g to 4 g. The peak serum level at 2 hours was 65 µg/mL and the drug serum half-life was 13.1 ± 4.0 hrs. A linear relationship was demonstrated between administered dose and serum level. Based on animal studies, a serum level of 100 µg/mL was considered necessary for effective radiosensitization and the oral dose calculated to achieve that serum level was 6.5 g. Single oral doses of 4-10 g were administered to 8 patients with advanced cancer and a life expectancy limited to 12 months. All patients experienced some degree of nausea, vomiting and anorexia for 24 hours. One of the eight had insomnia. At 10 g the nausea

and vomiting were extreme, and the anorexia lasted for a week. Peak serum levels were obtained between 1 and 3 hrs. The serum half-life ranged from 9-17 hrs with the median at 14 hrs.

Clinical studies employing multiple dosing of MISO have also been reported and peripheral neuropathy (PN) was the manifestation of toxicity that became dose limiting with daily doses of 3-5 g/m2. The results of a sequential dose reduction study[46] are shown in Table 6:

Table 6. Clinical toxicity of misonidazole

Dose (g/m^2)	Doses/wk.	Weeks	Affected Patients	Total Patients	% Pts. with peripheral neuropathy
3-5	5	3	12	16	75
2	2	3	2	6	33
0.4-0.8	3-5	3-6	1	6	16

This data demonstrates the dose proportionality of the drug's primary toxicity during chronic administration at doses that far exceed those used in PET imaging. Limiting the total dose and giving no more than two doses in one week minimized toxicity.

Significantly lower peripheral neuropathic (PN) toxicity for therapeutic doses has been observed with weekly dosing schedules: 1 of 12 with PN at 1-2g/m^2 for 6 weeks[47] and 0 of 10 at 3g/m^2 for 4 weeks[48]. This is presumably due to the fact that the drug, which has a long serum half-life, is allowed to clear completely from the body. Dische had a similar experience, noting that calculations by surface area produce the most consistent correlation of oral dose to plasma level and that the maximum recommended safe dose was 12 g/m^2 over no less than 18 days[49]. Neuropathies were generally, but not always, reversible when the drug was discontinued.

There have been two fatalities attributed to the drug[50]. Both patients had advanced malignant disease and died in convulsions: One patient received 51g in 6 fractions over 17 days, and the other patient received 16g in 2 doses over 3 days.

The above data supports the conclusion that FMISO's primary toxicity is likely to be peripheral neuropathy, which is dependent upon frequency and dose level. There is no evidence to suggest that FMISO poses a risk for PN when administered as an imaging agent for PET as described herein. The risk for PN in fact appears to be minimized or absent even at therapeutic doses that far exceed those necessary for PET imaging.

5. [^{19}F]FMISO HUMAN TOXICITY

A search for recent articles dealing with the human toxicity of fluoromisonidazole (FMISO) yields no results. Therefore, this assessment relies on animal studies and

similarities among related chemical entities. The octanol/water partition coefficients for MISO and FMISO are 0.43 and 0.41, respectively; the LD50's in adult male Balb/C mice for MISO and FMISO are 1.8 mg/g (1.3-2.6) and 0.9 mg/g, respectively[38] and in CH3 mice the LD50 is 0.6 mg/g for FMISO[39]. Using the relative toxicity factors from Paget (1962)[51] of 1.0 for mice and 9.8 for humans, the projected LD_{50} values are:

LD_{50} values	Misonidazole	Fluoromisonidazole
Concentration for human	0.184 g/kg	0.06-0.09 g/kg
Dose for 70 kg subject	12.86 g	6.43 g

The MISO values by this calculation are conservative when compared with the findings in early human trials (see Section 7, MISO Human Safety Studies). The serum half-lives of orally administered MISO and FMISO in mice were 2.3 hrs (range 1.87-2.92) and 2.0 hrs (range 1.79-2.24), respectively. The long component of the plasma half-life of FMISO in humans is similar to MISO (8-17 hrs). FMISO is cleared primarily through the kidneys.

The maximum dose to humans reported in imaging protocols was 1 mg/kg or 70 mg for a 70 kg subject; no adverse events have been reported. These studies are reported in Part VII. This is about 0.1% of the projected LD_{50}. Total patient imaging doses of the current radiopharmaceutical formulation contain ≤ 15 µg of fluoromisonidazole and less than 35 µg of other nitroimidazole derivatives. This is <0.001% of the projected LD50. The drug has had no toxic effects at these doses based upon a review of 5400 patients included in MISO studies[44] and over 269 patients studied with tracer doses of [^{18}F]FMISO, as summarized in this document (Section 9).

6. [^{18}F]FMISO HUMAN TOXICITY

Since the half-life of fluorine-18 is only 110 minutes, toxicity studies are not possible with the radiolabeled agent. The misonidazole data presented and the [^{19}F]FMISO calculations presented above in sections 4 and 5 should be the basis for both animal and human toxicity characterization and conclusions. The radiation dose associated with [^{18}F]FMISO is discussed separated in Part VI.

7. MISO HUMAN SAFETY STUDIES

Misonidazole for Therapy. In addition to their role as imaging agents, nitroimidazoles have been studied as therapeutic radiosensitizers (oxygen mimetics). These studies of over 7000 patients in 50 randomized trials have been reviewed[44]. Oral MISO was the agent in 40 of the trials involving about 5400 patients. The maximum doses used were 4 g/m^2 in a single dose and 12 g/m^2 as a total dose. The most common serious/dose limiting side effect was peripheral neuropathy with a latency period of several weeks.

The neuropathy was prolonged and, in some cases, irreversible. Nausea, vomiting, skin rashes, ototoxicity, flushing and malaise have also been reported at therapeutic dosing levels that vastly exceed imaging dose requirements. While these molecules are no longer used as clinical radiosensitizers, the results show the range of human experience with nitroimidazoles, and, in particular, support a reliable trend towards safety at imaging range dosing.

A 1978 study of oral misonidazole (MISO) as a radiosensitizing agent in human astrocytoma found good absorption, peak plasma levels between 1 and 4 hours and a half-life between 4.3 and 12.5 hours. Doses limited to 12 g/m^2 produced some nausea and vomiting but no serious side effects[48]. In an earlier study, Gray found a wide variation in tumor/plasma distribution ratios in six cases of advanced human metastatic breast cancers and soft tissue sarcomas[45]. The maximum dose in this study was 10 g, which caused a week of anorexia. Patients receiving up to 140 mg/kg tolerated the drug well.

8. [^{19}F]FMISO HUMAN SAFETY STUDIES

We are unaware of, nor did a literature search show, any human studies of [^{19}F]FMISO safety in humans beyond the carrier [^{19}F]-FMISO associated with the [^{18}F]FMISO human studies described below.

9. [^{18}F]FMISO HUMAN SAFETY STUDIES

[^{18}F]FMISO is a radiolabeled imaging agent that has been used for investigating tumor hypoxia with PET. It is composed of ≤ 15 µg of fluoromisonidazole labeled with ≤ 10 mCi of radioactive ^{18}F at a specific activity >1 Ci/mg at the time of injection. The drug is the only active ingredient and it is formulated in ≤ 10 mL of 5% ethanol in saline for intravenous injection. The radiochemical purity of the [^{18}F]FMISO is >95%.
Hypoxia imaging in cancer was reviewed in several recent publications[22,52,53,54]. [^{18}F]FMISO is a robust radiopharmaceutical useful in obtaining images to quantify hypoxia using PET imaging[55,56,57]. It is the most commonly used agent for PET imaging of tissue/tumor hypoxia[58,52,53,54,59,60,61].

Positron emission scanning with ^{18}F-FMISO has been studied over the past ten years in Australia, Switzerland, Denmark, Germany, China, and the United States under RDRC approval or its equivalent. Several published studies from the United States are from the University of Washington in Seattle and were conducted under an IND. Since 1994 up to 4 injections of FMISO, each followed by a PET scan, have been performed in Seattle alone on approximately 300 patients; data have been published on over 133 of these. [^{18}F]FMISO has been used to image ischemic stroke, myocardial ischemia and a wide variety of malignancies. Although, if totaled, the papers in Table 8 would list approximately 700 patients, we have taken a more conservative approach to reduce

possible duplication from multiple papers using the same patient data. Nonetheless as many as four ^{18}F-FMISO injections and PET scans have been performed in over 600 different patients represented in the published papers as listed in Part VII, "Previous Human Experience." Administered doses ranged from approximately 3 to 30 mCi (100-1100 MBq). As would be expected based upon the above safety assessment of the agent when dosed and used for imaging, no adverse events have been attributed to ^{18}F-FMISO in any of these reports.

10. FMISO GENOTOXICITY AND MUTAGENICITY

Multiple studies have found genetic transformations due to misonidazole and related nitroimidazoles using in vitro assays. The murine C3H/10T½ cell line (mouse embryo fibroblast) has a normal spontaneous transformation frequency of $<10^{-5}$ but these cells undergo oncogenic transformation in vitro when exposed to chemical and physical agents. The frequency of transformants with 3 days exposure to 1 mM drug was 2.27± 0.38 x 10^{-4} for FMISO and 4.55 ± 0.95 x 10^{-4} for misonidazole[62]. Although these values are about three to five times the background rate, this level of drug exposure would require about 10 grams of drug in a human. Imaging studies will inject ≤ 15 µg, or about 0.00015%.

FMISO and MISO were mutagenic when assayed by the AMES protocol using specific Salmonella typhimurium strains. MISO showed an increasing growth of revertants from 0 at 1 µg drug per plate to ~1500 at 100 µg per plate and ~6,000 at 1,000 µg per plate containing 0.1 mL of tester strain bacteria; FMISO showed fewer revertants, ~1,000 at 100 µg drug per plate and only ~600 revertants at 10 µg per plate[63]. In other cell lines, the frequency of unscheduled DNA synthesis was used as an index of genotoxicity. In this assay, [^{3}H]-thymidine incorporation in units of dpm/µg of DNA is used to quantify DNA synthesis. For a 1 mM dose of FMISO, the rate was 54 ± 6 for hepatocytes, 187 ± 14 for BL8 (nontransformed) cells and 217 ± 11 for JB1 (transformed) cells[64], with very similar values for MISO). For comparison, the control rate of DNA synthesis was 54 ± 4, 179 ± 15 and 158 ± 14, respectively for the three cell lines. This work concluded that in hypoxic cells nitroimidazoles react much more with thiols than with DNA. While each of these three tests detected low level alterations to DNA, exposure was both several orders of magnitude greater than, and of longer duration than that required in PET imaging with [^{18}F]FMISO. Drug exposure for imaging studies is below the levels where any genotoxicity was observed.

11. ADVERSE EVENTS AND MONITORING FOR TOXICITY

No adverse events have been attributed to PET imaging/diagnostic administration of [^{18}F] FMISO at the levels described herein in well over 1,000 injections, based upon up to 4 injections administered to each of over 600 patients. Thus no adverse effects are expected as a result of the IV administration of [^{18}F]FMISO for typical PET imaging

applications such as tumor hypoxia. The proposed [^{18}F]FMISO imaging dose is less than 0.001% of the recommended safe intravenous dose.

For purposes of informed consent regarding reasonably foreseeable risks to subjects in trials utilizing [^{18}F]FMISO, the following potential adverse effects are considered extremely rare:

- Risks related to allergic reaction that may be life threatening
- Injection related risks that may include infection, or extravasation of the dose that may lead to discomfort, localized pain, temporary loss of local function, and self limited tissue damage,

These risks are minimized by the requirement that appropriately trained and licensed/certified personnel prepare, deliver and administer the agent. The subject should be monitored per institutional standards for PET imaging studies. Emergency equipment, procedures, and personnel should be in place per institutional standards for imaging performed with intravenous contrast.

Radiation from ^{18}F carries an associated risk to the patient. The organ and total body doses associated with FMISO PET imaging are comparable to or lower than those associated with other widely used clinical nuclear medicine procedures and are well below the maximum individual dose suggested for investigational radiopharmaceuticals by the FDA.

12. SAFETY AND TOXICITY OF THE OTHER COMPONENTS OF THE FINAL [^{18}F]FMISO DRUG PRODUCT

The [^{18}F]FMISO is purified by HPLC using an eluent of 5% ethanol, USP. The injected dose is in up to 10 mL of 5% ethanol, or a maximum of 0.5 mL of ethanol. This is less than 5% of the amount of ethanol in one beer. In the Registry of Toxic Effects of Chemical Substances (RTECS) the LD_{Lo} for ethanol is given as 1.4 g/kg orally for producing sleep, headache, nausea and vomiting. Based upon widespread and routine use of ethanol in injectates, in concentrations and quantities similar to that specified herein, there is no reason to suspect that residual ethanol from [^{18}F]FMISO purification would pose any danger of toxicity when used in imaging studies.

The other components of the final product solution are USP grade sterile water for injection and sterile saline. These are all nontoxic for USP grade injectables at the concentrations used. The final product is at pH 7 and the final injection volume is ≤10 mL.

The potential contaminants in the final [^{18}F]FMISO drug product are: acetone, acetonitrile, Kryptofix® [2.2.2], other reaction products and if they are not required for

the system in use, they are not measured. Residual solvents in the final product are limited to 5,000 ppm (µg/mL) of acetone and 410 ppm of acetonitrile. Acetone is used to clean the TRACERLab FX_{F-N} and other related systems but not all new cassette based systems do. Acetonitrile is used to dissolve the Kryptofix® [2.2.2] and is the solvent for the reaction. The permissible level of acetonitrile in the final product is ≤400 ppm, the USP permissible level of acetonitrile in 2-[^{18}F]FDG. The allowable level for acetone is <5,000 ppm. Acetone is a Class three solvent. This class of solvents includes no solvent known as a human health hazard at levels normally accepted in pharmaceuticals. Therefore, this limit is based upon the FDA's Guidance for Industry ICH Q3C-Tables and List (November 2003 Revision 1), page 7, where it considers 5,000 ppm in 10 mL, 50 mg or less per day, of Class 3 residual solvents as an acceptable limit without additional justification.

The toxicity for Kryptofix® [2.2.2] has not been reported (RTECS Number Kryptofix® [2.2.2] MP4750000) although this reagent has been investigated as a therapeutic in mice for chelation therapy after strontium exposure. The FDA has proposed a maximum permissible level of 50µg/mL of Kryptofix® [2.2.2] in 2-[^{18}F]FDG, therefore this maximum permissible level will also apply to the [^{18}F]FMISO final product.

There are trace amounts of other reaction products in the final product. The principal trace impurity is 1-(2,3-dihydroxy)propyl-2-nitroimidazole but other impurities are possible. For this reason the upper limit is set at 35 µg for the total of other materials in the final injectate that are retained more than 3 minutes on C18 HPLC (Aquasil 2X150 mm at 0.3 mL/min) and have UV absorbance at 254, 280 or 327 nm. The 35 µg is determined by assuming that the UV absorbing compounds have the same molar extinction coefficient as FMISO.

VI. BIODISTRIBUTION AND RADIATION DOSIMETRY OF FMISO

^{18}F is a positron emitter with a half-life of 110 minutes. Intravenously injected [^{18}F]-FMISO distributes throughout the total body water space, crossing cell membranes, including the blood-brain-barrier, by passive diffusion. [^{18}F]FMISO is bound and retained within viable hypoxic cells in an inverse relationship to the O_2 concentration. The uptake of [^{18}F]FMISO in normal human tissues has been measured and used to estimate the radiation absorbed dose associated with the imaging procedure. Dosimetry studies were performed at the University of Washington and have been published in the peer-reviewed Journal of Nuclear Medicine[55].

Sixty men and women were subjects in the study. Of these, 54 had cancer, three had a history of myocardial ischemia, two were paraplegic and one had rheumatoid arthritis. After injecting 3.7 MBq/kg (0.1 mCi/kg), urine and normal tissues distant from each subject's primary pathology were imaged repeatedly to develop time-activity curves for target tissues. All tissues demonstrated a rapid uptake phase and first-order near-logarithmic clearance curves. All tissues receive a similar radiation dose, reflecting the

similarity of biodistribution to that of water. Total tissue uptake data were normalized for a 1.0 MBq injection into a 70 kg man. The organ curves are shown in Figure 4 and Figure 5[55]:

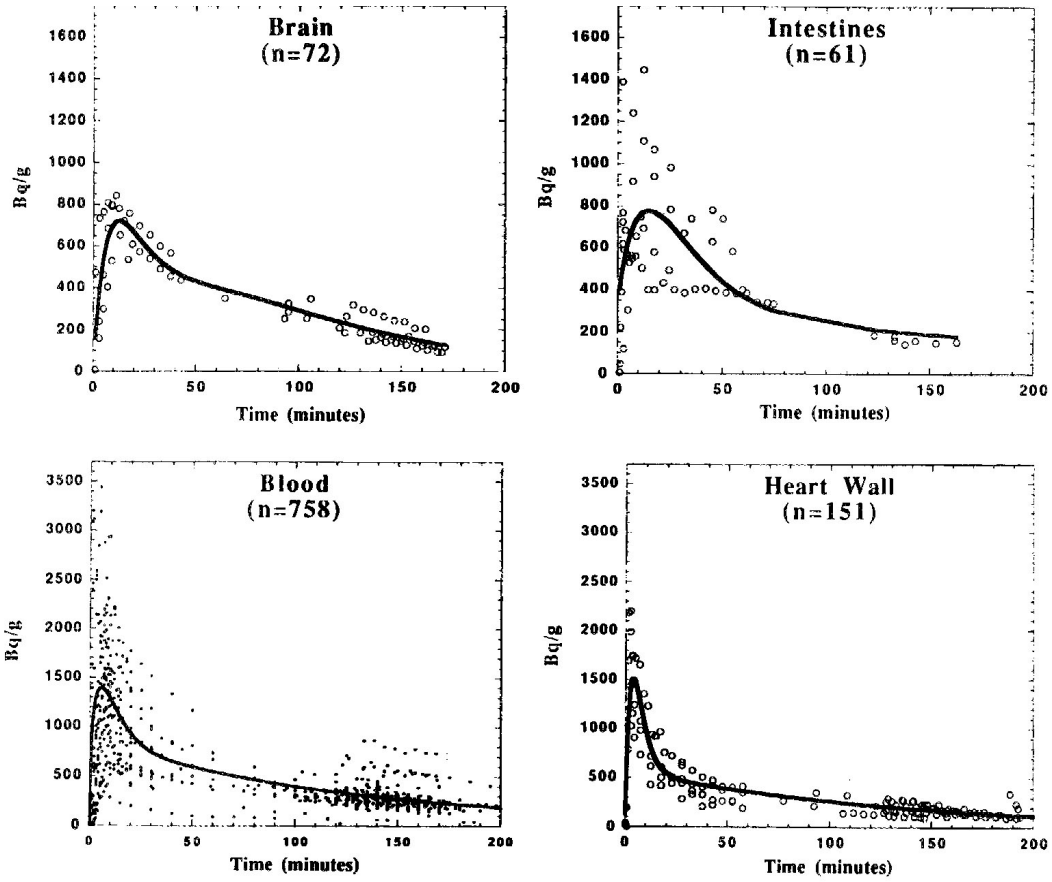

Figure 4. Activity of FMISO in 4 source organs with best fit used to determine AUC. The data are normalized to 1 MBq/70 kg bw.

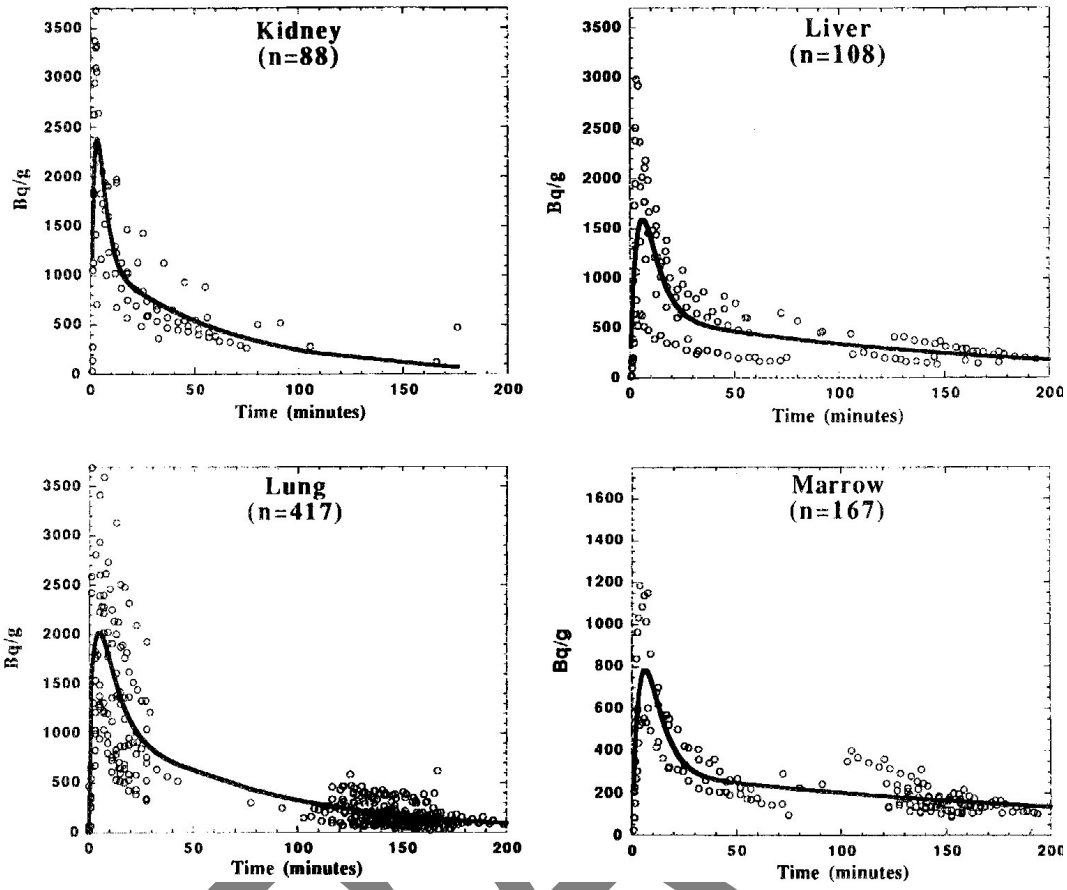

Figure 5. Activity of FMISO in four other source organs with best fit used to determine AUC. The data are normalized to 1 MBq/70 kg bw.

Radiation dose to the bladder wall varied with voiding interval from 0.021-0.029 mGy/MBq. *Figure 6*[55] is a composite of the integrated ^{18}F urine activity of 42 samples from 20 studies. The line is the best fit to the data and was used to determine AUC for individual patients. Note that the mean total excretion is about 30 kBq, or 3% of the injected dose.

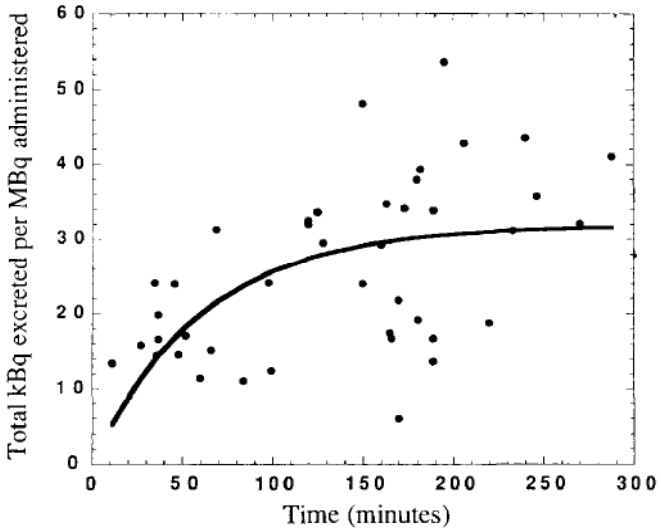

Figure 6. Bladder activity from injection of 1 MBq of [^{18}F]FMISO/ 70 kg bw.

From these human data, radiation absorbed doses to organs was calculated using the MIRD schema and the results are shown in Table 7[55].

Table 7. Radiation Absorbed Dose to Organs

Tissue	Mean (mGy/MBq)	Mean (mrad/mCi)	Total / 7 mCi (mrad)
adrenals	0.0166	61.4	430
Brain	0.0086	31.8	223
Breasts	0.0123	45.5	319
gall bladder wall	0.0148	54.8	383
lower large intestine	0.0143	52.9	370
small intestine	0.0132	48.8	342
stomach	0.0126	46.6	326
upper large intestine	0.0140	51.8	363
heart wall	0.0185	68.5	479
kidneys	0.0157	58.1	407
Liver	0.0183	67.7	474
Lungs	0.0099	36.6	256
Muscle	0.0142	52.5	368
Ovaries	0.0176	65.1	456
pancreas	0.0179	66.2	464
red marrow	0.0109	40.3	282
bone surface	0.0077	28.5	199
Skin	0.0048	17.8	124
Spleen	0.0163	60.3	422
Testes	0.0146	54.0	378
Thymus	0.0155	57.4	401
Thyroid	0.0151	55.9	391
urinary bladder wall	0.0210	77.7	544
Uterus	0.0183	67.7	474
eye lens	0.0154	57.0	399
Total body	0.0126	46.6	325

Calculated total body dose for a 70 kg man injected with 3.7 MBq/kg was 0.013 mGy/MBq; for a 57 Kg woman it was 0.016 mGy/MBq. Effective dose equivalents were 0.013 mSv/MBq for men and 0.014 mSv/MBq for women. Ninety-seven percent of the injected radiation was homogenously distributed in the body, leaving only 3% for urinary excretion. Doses to smaller organs not directly determined by visualization, such as the lens, were calculated assuming average total-body concentrations. The absence of tracer visualized in images of those organs indicated that accumulation there was not increased.

The radiation exposure from [^{18}F]FMISO is equal to or lower than that of other widely used nuclear medicine studies. Increasing the frequency of voiding can reduce radiation dose to the normal organ receiving the highest radiation absorbed dose, the bladder

wall. Potential radiation risks associated with a typical PET study utilizing this agent are within generally accepted limits.

Additional radiation exposure will occur with any PET study, but is site and procedure specific. Attenuation correction is required, from either a germanium rod transmission or a low dose CT scan. The radiation dose is larger with CT attenuation correction and larger for body compared to head, but will depend on the exact equipment and scanning protocol used. Each trial site will need to address this with their local information.

VII. [^{18}F]FMISO PREVIOUS HUMAN EXPERIENCE AND ASSESSMENT OF CLINICAL POTENTIAL

[^{18}F]FMISO is a radiolabeled imaging agent that has been used for investigating tumor hypoxia with PET. A hypoxia-imaging agent should be independent of blood flow, which is achieved when the partition coefficient of the tracer is close to unity and imaging is done at a time when the tracer distribution has equilibrated with its entry into the cells. [^{18}F]FMISO is an azomycin-based hypoxic cell sensitizer that has a nearly ideal partition coefficient and binds covalently to molecules at rates that are inversely proportional to intracellular O_2 concentration, rather than by some downstream biochemistry. It is composed of ≤ 15 µg of fluoromisonidazole labeled with ≤ 10 mCi of radioactive ^{18}F at a specific activity ≥1 Ci/mg at the time of injection. The drug is the only active ingredient and it is formulated in ≤ 10 mL of 5% ethanol in saline for intravenous injection. The radiochemical purity of the [^{18}F]FMISO is ≥ 95%.

Hypoxia imaging in cancer was reviewed in several publications[22,52,53,54,65]. [^{18}F]FMISO is a robust radiopharmaceutical useful in obtaining images to quantify hypoxia using PET imaging[55,56,57]. It is the most commonly used agent for PET imaging of hypoxia [58,52,53,54,59,60,61]. While its biodistribution properties do not result in high contrast images, they result in images at approximately 2 hours after injection that unambiguously reflect regional partial pressure of oxygen, Po_2, and hypoxia in the time interval after the radiopharmaceutical was administered.

Positron emission scanning with [^{18}F]FMISO has been studied over the past ten years in Australia, Switzerland, Denmark, Germany and in the United States under RDRC approval or its equivalent. Several published studies from the United States are from the University of Washington in Seattle and were conducted under IND 32,353. Since 1994, approximately 300 patients have undergone FMISO PET scans in Seattle, at least 133 of whom are included in Table 8 of published studies. [^{18}F]FMISO has been used to image ischemic stroke, myocardial ischemia, and a wide variety of malignancies.

Based upon published papers we know, over 3,900 unique patients have undergone up to 4 injections of the agent as described herein. Administered doses ranged from

approximately 3 to 30 mCi (100 - 1100 MBq). No adverse events were noted in any of these papers, which are summarized in *Table 8.* Representative recent papers from key groups in [F-18]FMISO PET imaging are summarized below.

In a paper published by Mortensen in 2010[65] 18 F-FMISO PET was compared to polarographic oxygen-sensitive electrodes. The aim of this study was to examine the association between measures of hypoxia defined by functional imaging and Eppendorf pO 2 electrodes. Nine patients with squamous cell carcinoma of the head and neck and nine with soft tissue tumors were included. The tumor volume was defined by CT, MRI, 18 FDG-PET or by clinical examination. The oxygenation status of the tumors was assessed using 18 F-FMISO PET imaging followed by Eppendorf pO2 electrode measurements. Data were compared in a `virtual voxel`, resulting in individual histograms from each tumor. For 18 F-FMISO PET the T/M ratio ranged from 0.70 to 2.38 (median 1.13). Analyzing the virtual voxel histograms, tumors could be categorized in three groups: Well oxygenated tumors with no hypoxia and concordance between the 18 F-FMISO data and the Eppendorf measurements, hypoxic tumors likewise with concordance between the two assays, and inconclusive tumors with no concordance between the assays. The conclusion was that there was a spectrum of hypoxia among tumors that can be detected by both assays. However no correlation was observed, and in general, tumors were more hypoxic based on Eppendorf pO 2 measurements as compared to 18 F-FMISO PET.

In a paper published in 2009, Swanson[190] reported on 24 patients with glioblastoma who underwent T1Gd, T2, and 18F-FMISO studies either prior to surgical resection or biopsy, after surgery but prior to radiation therapy, or after radiation therapy. Abnormal regions seen on the MRI scan were segmented, including the necrotic center (T0), the region of abnormal blood-brain barrier associated with disrupted vasculature (T1Gd), and infiltrating tumor cells and edema (T2). The 18F-FMISO images were scaled to the blood 18F-FMISO activity to create tumor-to-blood ratio (T/B) images. The hypoxic volume (HV) was defined as the region with T/Bs greater than 1.2, and the maximum T/B (T/Bmax) was determined by the voxel with the greatest T/B value. They found that the HV generally occupied a region straddling the outer edge of the T1Gd abnormality and into the T2. A significant correlation between HV and the volume of the T1Gd abnormality that relied on the existence of a large outlier was observed. There was consistent correlation between surface areas of all MRI-defined regions and the surface area of the HV. The T/Bmax, typically located within the T1Gd region, was independent of the MRI-defined tumor size. Univariate survival analysis found the most significant predictors of survival to be HV, surface area of HV, surface area of T1Gd, and T/Bmax. They concluded that hypoxia may drive the peripheral growth of glioblastomas[147].

In a 2008 paper by Lin, seven patients with head and neck cancers were imaged twice with FMISO PET, separated by 3 days, before radiotherapy. Intensity-modulated radiotherapy plans were designed, on the basis of the first FMISO scan, to deliver a

boost dose of 14 Gy to the hypoxic volume, in addition to the 70-Gy prescription dose. The same plans were then applied to hypoxic volumes from the second FMISO scan, and the efficacy of dose painting evaluated by assessing coverage of the hypoxic volumes using Dmax, Dmin, Dmean, D95, and equivalent uniform dose (EUD). The authors found similar hypoxic volumes in the serial scans for 3 patients but dissimilar ones for the other 4. There was reduced coverage of hypoxic volumes of the second FMISO scan relative to that of the first scan. The decrease was dependent on the similarity of the hypoxic volumes of the two scans. They concluded that the changes in spatial distribution of tumor hypoxia, as detected in serial FMISO PET imaging, compromised the coverage of hypoxic tumor volumes achievable by dose-painting IMRT. However, dose painting always increased the EUD of the hypoxic volumes[193].

In a study published in 2008, Roels et al. investigated the use of PET/CT with fluorodeoxyglucose (FDG), fluorothymidine (FLT) and fluoromisonidazole (FMISO) for radiotherapy (RT) target definition and evolution in rectal cancer. PET/CT was performed before and during preoperative chemoradiotherapy (CRT) in 15 patients with resectable rectal cancer. They concluded that FDG, FLT and FMISO-PET reflect different functional characteristics that change during CRT in rectal cancer. FLT and FDG show good spatial correspondence, while FMISO seems less reliable due to the non-specific FMISO uptake in normoxic tissue and tracer diffusion through the bowel wall. FDG and FLT-PET/CT imaging seem most appropriate to integrate in preoperative RT for rectal cancer[198].

Nehmeh et al. reported a study on 20 head and neck cancer patients in a 2008 paper. Of these, 6 were excluded from the analysis for technical reasons. All patients underwent an FDG study, followed by two (18)F-FMISO studies 3 days apart. The authors found that variability in spatial uptake can occur between repeat (18)F-FMISO PET scans in patients with head and neck cancer. Of 13 patients analyzed, 6 had well-correlated intratumor distributions of (18)F-FMISO-suggestive of chronic hypoxia. They concluded that more work is required to identify the underlying causes of changes in intratumor distribution before single-time-point (18)F-FMISO PET images can be used as the basis of hypoxia-targeting intensity-modulated radiotherapy[197].

In a 2008 paper Lee reported on a study that examined the feasibility of ((18)F-FMISO PET/CT)-guided IMRT with the goal of maximally escalating the dose to radioresistant hypoxic zones in a cohort of head and neck cancer (HNC) patients. (18)F-FMISO was administered intravenously for PET imaging. The CT simulation, fluorodeoxyglucose PET/CT, and (18)F-FMISO PET/CT scans were co-registered using the same immobilization methods. The tumor boundaries were defined by clinical examination and available imaging studies, including fluorodeoxyglucose PET/CT. Regions of elevated (18)F-FMISO uptake within the fluorodeoxyglucose PET/CT GTV were targeted for an IMRT boost. Additional targets and/or normal structures were contoured or transferred to treatment planning to generate (18)F-FMISO PET/CT-guided IMRT plans. The authors

found that the heterogeneous distribution of (18)F-FMISO within the GTV demonstrated variable levels of hypoxia within the tumor. Plans directed at performing (18)F-FMISO PET/CT-guided IMRT for 10 HNC patients achieved 84 Gy to the GTV(h) and 70 Gy to the GTV, without exceeding the normal tissue tolerance. An attempt to deliver 105 Gy to the GTV(h) for 2 patients was successful in 1, with normal tissue sparing. The conclusion was that it was feasible to dose escalate the GTV(h) to 84 Gy in all 10 patients and in 1 patient to 105 Gy without exceeding the normal tissue tolerance. This information has provided important data for subsequent hypoxia-guided IMRT trials with the goal of further improving locoregional control in HNC patients[195].

Thorwarth et al. published a 2008 paper on a dose painting strategy to overcome hypoxia-induced radiation resistance. 15 HNC patients were examined with 18F-FDG and dynamic 18F-FMISO PET before the start of a 70Gy radiotherapy. After approx. 20 Gy, a second dynamic 18F-FMISO scan was performed. The voxel based 18F-FMISO PET data were analyzed with a kinetic model, which allows for the determination of local tumor parameters for hypoxia and tissue perfusion. Their statistical analysis showed that only a combination of these two parameters predicted treatment outcome. They concluded that a translation of the imaging data into a reliable dose prescription can only be reached via a TCP model that includes these functional parameters. A model was calibrated using the outcome data of the 15 HNC patients. This model mapping of locally varying dose escalation factors to be used for radiotherapy planning. A planning study showed that hypoxia dose painting is feasible without a higher burden for the organs at risk[196].

Table 8. Published manuscripts reporting 18F-FMISO human imaging studies

Year	Clinical Condition	N	mCi injected	MBq injected	Reference
2021	Adenocarcinoma (Biliary tract cancer)	20	15 mCi	555 MBq	Yoon[66] (Korea 2021)
2021	Head and Neck Squamous Cell Carcinomas	8	0.1 mCi	3.7 MBq/kg),	Rogasch[67] (Germany 2021)
2021	Lung	20	0.12 mCi/kg	4 MBq/kg	Thureau[68] (France 2021)
2021	Glioma	87	7.1 ± 1.5 mCi	262 ± 54.3 MBq	Suzuki[69] (Japan 2021)
2021	Head-and Neck	39			Rühle[70] (Germany 2021)
2021	Head and Neck Squamous Cell Carcinomas	23	10.5 ± 0.4 mCi1	390 ± 16 MBq	Paudyal[71] (USA 2021)
2021	head and neck squamous cell	20	10.5 mCi	387.8 MBq	Nehmeh[72] (USA 2021)
2021	Breast	70			López-Vega[73] (Spain 2021)
2021	colorectal carcinoma	15	10 mCi	370 MBq	Lee[74] (Australia 2021)
2021	Colorectal Carcinoma	40	10 mCi	370 MBq	Lee[75] (Australia 2021)
2021	Head & Neck Squamous Cell Carcinoma	28	8.1 mCi 8.2 ± 0.6 mCi	300 MBq 303 ± 21 MBq	Lazzeroni[76] (Sweden 2021)
2021	Glioblastoma	33	0.1 mCi/kg	3.7 MBq/kg	Huang[77] (USA 2021)
2021	Glioblastoma	20	0.1 mCi	5 MBq	Collet[78] (France 2021)
2021	Breast	29	8.3 ± 0.4 mCi	306 ± 14 MBq	Carmona-Bozo[79] (UK 2021)
2021	head and neck squamous cell carcinoma	50			Zschaeck[80] (Germany 2021)

2021	Head-and-Neck	35	0.12 mCi/kg	4 MBq/kg	Carles[81] (Germany 2021)
2020	Head & Neck	196	6.7 – 12 mCi	250 – 444 MBq	Socarrás Fernándeza[82] (Germany 2020)
2020	Glioblastoma	10	0.05 mCi/KG	1.85 MBq/kg	Leimgruber[83] (Australia 2020)
2020	Head and Neck Squamous Cell	49	0.1 mCi/kg	3.7 MBq/kg to a	Nicolay[84] (Germany 2020)
2020	Head and Neck Squamous Cell	49	0.1 mCi/KG	3.7 MBq/kg	Rühle[85] (Germany 2020)
2020	oral squamous	18			Shima[86] (Japan 2020)
2020	head and neck squamous cell carcinoma	29	0.12 ± 0.03 mCi/kg	4.4 ± 1.0 MBq/kg	Sörensen[87] (Germany 2020)
2020	Non-small-cell Lung	79	0.12 mCi/kg	4.5 MBq/kg	Thureau[88] (France 2020)
2020	head and neck	21	5.6–9.0 mCi	209–332 MBq	Wiedenmann[89] (Germany 2020)
2020	head and neck	102			Zschaeck[90] (Germany 2020)
2019	Breast	9	0.08 mCi	3 MBq	Andrzejewski[91] (USA 2019)
2019	Head & Neck Squamous Cell Carcinoma	45			Bandurska-Luque[92] (Germany 2019)
2019	Head & Neck	36	5 ± 2.03 mCi	185 ± 75 MBq	Cegla[93] (Poland 2019)
2019	Myocardium	26	0.1 mCi/kg	3.7 MBq/kg	Jagtap[94] (India 2019)
2019	Head-and-Neck	38	10.8 mCi	400 MBq	Kroenke[95] (Japan 2019)
2019	Head and neck squamous cell carcinomas	50	6.7 – 8.12 mCi	250–300 MBq	Löck[96] (Germany 2019)

2019	Non–Small	21	10 mCi	370 MBq	McGowan[97] (United Kingdom 2019)
2019	Brain	15	0.1 mCi/kg	5 MBq/kg	Shimizu[98] (Japan 2019)
2019	Prostate Cancer	9	0.08 mCi/kg	3 MBq/kg	Supiot[99] (France 2019)
2019	Head & Neck	25			Thorwarth[100] (Germany 2019)
2019	Non Small Cell Lung	54			Vera[101] (France 2019
2019	Non Small Cell Lung	32	10.8 mCi	400 MBq	Watanabe[102] (Japan 2019)
2019	Pancreatic Adenocarcinoma	25	0.2 mCi/kg	7.4 MBq/kg	Yamane[103] (Japan 2019)
2019	Gliomas	9	0.1 mCi/kg	3.7 MBq/kg	Abdo[104] (France 2019)
2019	Brain	23	10.7 mCi	395.0 MBq	Kobayashi[105] (Japan 2019)
2018	non-small cell lung	5			Li[106] (China 2018)
2018	Non-small Cell Lung	29	0.13 mCi/kg	4.81 MBq/kg	Li[107] (China 2018)
2018	Non-Small Cell Lung	21			Thureau[108] (France 2018)
2018	Head & Neck Squamous Cell Carcinoma	10	6.6–9.0	243–332	Wiedenmann[109] (Germany 2018)
2018	Radiotherapy	22	0.2 mCi/kg	7.4 MBq/kg	Tachibana[110] (Japan 2018)
2018	Prostate	27	0.08 mCi/kg	3 MBq/kg	Supiot[111] (France 2018)
2018	Oral Squamous Cell Carcinoma	23	10.8	400	Sato[112] (Jaban 2018)

2018	Glioblastoma	17	0.1 mCi/kg	3.7 MBq/kg	Ratai[113] (USA 2018)
2018	Non–Small Cell Lung Cancer	23	10.5-11	388–407	Nehmeh[114] (USA 2018)
2018	Non–Small Cell Lung Cancer	9	10	370	McGowan[115] (UK 2018)
2018	Non–Small Cell Lung Cancer	29	0.13 mCi/kg	4.81 MBq/kg	Li[116] (China 2018)
2018	Non–Small Cell Lung Cancer	5			Li[117] (China 2018)
2018	Head & Neck Squamous Cell Carcinoma	75			Crispin-Ortuzar[118] (USA 2018)
2018	Head & Neck Squamous Cell Carcinoma	18	0.095 mCi/kg	3.5 MBq/kg	Chatterjee[119] (India 2018)
2018	Breast	44	0.2 mCi/kg	7.4 MBq/kg	Asano[120] (Japan 2018)
2017	Head & Neck Squamous Cell Carcinoma	16	6.5–10.3	242–382	Schwartz[121] (USA 2017)
2017	Locally Advanced Squamous Cell Carcinomas of the Head and Neck	25			Welz[122] (Germany 2017)
2017	Breast	28	0.2 mCi/kg	7.4 MBq/kg	Ueda[123] (Japan 2017)
2017	Glioblastoma	32	11.1±0.76	413.9±28.2	Toyonaga[124] (Japan 2017)
2017	Head & Neck Squamous Cell Carcinoma	6	8.6-10.2	320-377	Simoncic[125] (Germany 2017)
2017	Oral Squamous Cell Carcinoma	23	10.8	400	Sato[126] (Japan 2017)
2017	nasopharyngeal cancer	8	10	370	Qiu[127] (China 2017)
2017	Rectal	11	9-10.7	333-397	Puri[128] (UK 2017)

2017	Glioblastoma	12	5.2± 0.95	194.6 ± 35.0	Preibisch[129] (Germany 2017)
2017	nasopharyngeal cancer	31	10.8	400	Nishikawa[130] (Japan 2017)
2017	Head & Neck Squamous Cell Carcinoma	25	8.5-12	315-444	Monnich[131] (Germany 2017)
2017	Non–Small Cell Lung Cancer	9	10	370	McGowan[132] (UK 2017)
2017	Head & Neck Squamous Cell Carcinoma	25	6.8-8.1	250-300	Lock[133] (Germany 2017)
2017	Non–Small Cell Lung Cancer	6	5	185	Kelada[134] (USA 2017)
2017	Glioblastoma	41	11.9±2.7	439.6±99.9	Kanoto[135] (Japan 2017)
2017	Head & Neck Squamous Cell Carcinoma	120	10.5 ±0.4	389 ± 15	Grkovski[136] (USA 2017)
2017	Head & Neck Squamous Cell Carcinoma	72	10.5 ± 0.4	390 ± 14	Grkovski[137] (USA 2017)
2017	Cervical	13	5.4-9.5	200–350	Georg[138] (USA 2017)
2017	Cervical	10	0.08 mCi/kg	3.0 MBq/kg	Daniel[139] (2017 Austria)
2017	Glioblastoma	23	0.14 mCi/kg	5.0 MBq/kg	da Ponte[140] (France 2017)
2017	Glioma	13	0.14 mCi/kg	5.0 MBq/kg	Chakhoyan[141] (France 2017)
2017	Head & Neck Squamous Cell Carcinoma	9			Boeke[142] (Germany 2017)
2017	Glioma	33	0.14 mCi/kg	5.0 MBq/kg	Bekaert[143] (France 2017)
2016	Lung	42	0.13 mCi/kg	4.81 MBq/kg	Wei[144] (China 2016)

2016	Breast	107	7.2± 0.4	267 ± 15.3	Quintela-Fandino[145] (Spain 2016)
2016	Advanced Human Papillomavirus	33	8-10	296-370	Lee[146] (USA 2016)
2016	Non–Small Cell Lung Cancer	10	9.6-11	356–407	Grkovski[147] (USA 2016)
2016	Head & Neck Squamous Cell Carcinoma	16	0.1 mCi/kg	3.7 MBq/kg	Bittner[148] (Germany 2016)
2016	Glioma	4	7	259	Barajas[149] (USA 2016)
2015	Non–Small Cell Lung Cancer	1	4.9	181	Zheng[150] (USA 2015)
2015	Non–Small Cell Lung Cancer	13	6.8	250	Sachpekidis[151] (Germany 2015)
2015	Glioma	1	7	259	Barajas[152] (USA 2015)
2015	Non–Small Cell Lung Cancer	2	9.5-10.5	352-389	Arvold[153] (USA 2015)
2014	Breast	7	0.2 mCi/kg	7.4 MBq/kg	Ueda[154] (UK 2014)
2014	Oral Squamous Cell Carcinoma	22	10.8	400	Sato[155] (Japan 2014)
2014	Glioblastoma	1			Rockne[156] (USA 2014)
2014	Stroke	19	15	555	Lee[157] (Korea 2014)
2014	Head & Neck Squamous Cell Carcinoma	10	0.1 mCi/kg	3.7 MBq/kg	de Figueiredo[158] (France 2014)
2013	Non–Small Cell Lung Cancer	5	0.05 mCi/kg	2.0 MBq/kg	Thereau[159] (France 2013)
2013	Various	10	0.2 mCi/kg	7.4 MBq/kg	Tachibana[160] (Japan 2013)

2013	Pancreatic	10	0.19 mCi/kg	7 MBq/kg	Segard[161] (Australia 2013)
2013	Oral Squamous Cell Carcinoma	23	10.8	400	Sato[162] (Japan 2013)
2013	Head & Neck Squamous Cell Carcinoma	11	11.2 ± 0.7	414 ± 26	Okamoto[163] (Japan 2013)
2013	Head & Neck Squamous Cell Carcinoma	39	0.1 mCi/kg	3.7 MBq/kg	Norikane[164] (Japan 2013)
2013	Head & Neck Squamous Cell Carcinoma	15	0.1 mCi/kg	3.7 MBq/kg	de Figueiredo[165] (France 2013)
2013	Head & Neck Squamous Cell Carcinoma	8	10	370	Chang[166] (China 2013)
2013	Head & Neck Squamous Cell Carcinoma	16	0.1 mCi/kg	3.7 MBq/kg	Bittner[167] (USA 2013)
2013	Stroke	3	0.05mCi/kg	1.85 MBq/kg	Alawneh[168] (UK 2013)
2012	Glioma	2	12.2	450	Narita[169] (Japan 2012)
2012	Head & Neck Cancer	7	10	370	Toma-dasu[170] (Belgium 2012)
2012	Glioma	23	10.8	400	Hirata[171] (Japan 2012)
2012	Glioma	30	0.1 mCi/kg Max 7	3.7 MBq/kg Max 260	Yamamoto[172] (Japan 2012)
2012	Skull Base Chordoma	7	0.14 mCi/kg	5 MBq/kg	Mammar[173] (France 2012)
2012	Head & Neck Cancer	40	10.8	400	Yasuda[174] (Japan 2012)
2012	Head & Neck Cancer	12	0.2 + 0.05 mCi/kg	7.3 $\pm$ 1.7 MBq/kg	Chen[175] (USA 2012)
2012	Head & Neck Cancer	25	6.8-8.1	250-300	Zips[176] (Germany 2012)
2012	Various cancers	17	0.1 mCi/kg <10	3.7 MBq/kg <370	McKeage[177] (New Zealand 2012)
2011	Glioma	10	5.3-9.4 Median = 8.3	197-348 Median = 308	Kawai[178] (Japan 2011)

2011	Non-Small Cell Lung Cancer	5	0.05 mCi/kg	2.0 MBq/kg	Vera[179] (France 2011)
2011	Sarcoma	10	7	259	Eary[180] (USA 2011)
2011	Head & Neck Squamous Cell Carcinoma	17	13.7-19.4 Mean 16	510-718 Median=592	Kikuchi[181] (Japan 2011)
2011	Head & Neck Cancer	10	0.1 mCi/kg Max 7	3.7 MBq/kg Max 370	Hendrickson[182] (USA 2011)
2011	Glioma	1	8.3	307	De Clermont[183] (France 2011)
2011	Renal Cell Carcinoma	53	0.14 mCi/kg	5 MBq/kg	Hugonnet[184] (France 2011)
2011	Head and Neck Cancer	23	6.9	256 ± 37	Abolmaali[185] (Germany 2011)
2011	Head & Neck Squamous Cell Carcinoma	13	13.7-19.4 Mean 16	510-718 Median= 592	Yamane[186] (Japan 2010)
2010	Head & Neck Cancer	8	20	740	Choi[187] (Korea 2010)
2010	Head & Neck Squamous Cell Carcinoma	9	10	370	Wang[188] (USA 2010)
2010	Soft Tissue & H & N	18	10.8 5.9 - 12.5	400 218 – 462	Mortensen[65] (Denmark 2010)
2009	Brain Cancer	11	0.1 mCi/kg 7 mCi	3.7 mCi/kg 260	Szeto[189] (USA 2009)
2009	Brain Cancer	24	0.1 mCi/kg 7 mCi	3.7 mCi/kg 260	Swanson[190] (USA 2009)
2009	Head & Neck Cancer	28	10	370	Lee[191] (USA 2009)
2008	Brain Cancer	22	0.1 mCi/kg 7 mCi	3.7 mCi/kg 260	Spence[192] (USA 2008)
2008	Head & Neck Cancer	7	10	370	Lin[193] (USA 2008)
2008	Head & Neck Cancer	15	Not Reported	Not Reported	Thorwarth[194] (Germany 2008)
2008	Head & Neck Cancer	28	9.3-11	344-407	Lee[195] (USA, 2008)
2008	Head & Neck Cancer	3	~10.8	~400	Thorwarth[196] (Germany, 2008)

2008	Head & Neck Cancer	20	9.3-11	344-407	Nehmeh[197] (USA, 2008)
2008	Rectal Cancer	10	8.9-11	330-398	Roels[198] (Belgium 2008)
2007	Advanced Head & Neck Cancer	14	9.4-12.2	350-450	Eschmann[199] (Germany 2007)
2007	Advanced Non-Small Cell Lung Cancer	4	7	259	Spence[200] (USA, 2007)
2007	Head & Neck Cancer	38	9.6	356	Gagel[201] (2007 Germany)
2007	Head & Neck Cancer	13	10.8	400	Thorwarth[202] (Germany 2007)
2006	Head & Neck	24	9.7 ± 0.7	360 ± 25	Zimny[203] (Germany 2006)
2006	Non-small cell lung cancer	21	10	370	Cherk[204] (Australia 2006)
2006	Head and Neck Cancer	45	Not Reported	Not Reported	Rischin[205] (Australia 2006)
2006	Head and Neck Cancer	73	Nominally 7.0 Max 10	Nominally 260 Max 370	Rajendran[206] (USA 2006)
2006	Non-Small Cell Lung Cancer	8	8.9 ± 0.10	329 ± 36	Gagel[207] (Germany, 2006)
2006	Glioma	17	0.05 mCi/kg	18.5 MBq/kg	Cher[208] (Australia 2006)
2005	Head & Neck cancer	26	9.4-12.2	350-450	Eschmann[60] (Germany 2005)+
	Non-Small Cell Lung Cancer	14			
2004	Various brain tumors	11	3.3-11.4 Average = 7.8	123-421 Average = 291	Bruehlmeier [209] (Switzerland 2004)
2004	Various cancers	49	0.1 mCi/kg	3.7/Kg nom 260	Rajendran[54] (USA 2004)
2004	Head & Neck cancer	16	7.9 ± 0.9	292 ± 35	Gagel[210] (Germany 2004)
2003	Ischemic Stroke	19	nom 3.5	nom 130	Markus[211] (Australia, 2003)
2003	Soft tissue tumors	13	5.9-11.3 Average= 10.8	218-418 Average= 400	Bentzen[212] (Denmark 2003)
2003	Soft Tissue Sarcoma	29	0.1 mCi/kg nom 7	3.7 MBq/kg nom 260	Rajendran[213] (USA 2003)

2000	Ischemic Stroke	24	nom 3.5	nom 130	Read[214] (Australia 2000)
1996	Various cancers	37	0.1 mCi/kg nom 7	3.7 MBq/kg nom 260	Rasey[215] (USA 1996)
1995	Non-Small Cell Lung Cancer	7	0.1 mCi/kg nom 7	3.7 MBq/kg nom 260	Koh[53] (USA 1995)
1992	Various cancers	8	0.1 mCi/kg	3.7 MBq/kg	Koh[216] (USA 1992)
1992	Glioma	3	~10	~370	Valk[59] (USA 1992)
	Total No. Subjects	**3,904***			

*It is possible that some patients are represented more than once.

The overall conclusion, based upon the studies summarized above, is that [^{18}F]FMISO PET identifies hypoxic tissue that is heterogeneously distributed within human tumors[215]. It promises to help facilitate image-guided radiotherapy and to also guide the use of hypoxia-selective cytotoxins. These are two ways, out of several, that this agent might potentially help circumvent the cure-limiting effects of tumor hypoxia. In addition, [^{18}F]FMISO has identified a discrepancy between perfusion, blood-brain barrier disruption, and hypoxia in brain tumors[209] and a lack of correlation between FDG metabolism and hypoxia in several types of malignancies[213]. Hypoxic tissue also does not correlate either with tumor volume or vascular endothelial growth factor (VEGF) expression[22,54].

[^{18}F]FMISO PET was able to identify post-radiotherapy tumor recurrence by differential uptake of tracer. The standardized uptake value (SUV) ratio between recurrent tumor and muscle was >1.6, while that between tumor and normal mediastinum was >2.0[60]. One study concluded that [^{18}F]FMISO was not feasible for the detection of tumor hypoxia in human soft tissue tumors[212]. In ischemic stroke, [^{18}F]-FMISO was able to identify the areas of brain tissue into which a stroke had extended[211,214]. In addition to the FMISO imaging studies summarized above, alternative nitroimidazoles have been evaluated as imaging agents in single-center pilot studies. A 2001 study from Finland used [^{18}F]-fluoroerythro-nitroimidazole ([^{18}F-FETNIM) to evaluate 8 patients with head and neck squamous cell cancer at doses of ~370 MBq without adverse effect[217] (Lehtio 2001). Other agents, fluoropropyl-nitroimidazole and fluorooctyl-nitroimidazole. have not proved as useful in visualizing hypoxic tissue[218] (Yamamoto 1999), probably because of their higher lipophilicity. A derivative that is more hydrophilic than FMISO, [^{18}F]-fluoroazomycin-arabinofuranoside (FAZA) had been recommended for further study[219] (Sorger 2003) and shows considerable clinical promise.

In human metastatic neck lymph nodes, comparison of FMISO tumor-to-muscle uptake ratio at 2 hours using the computerized polarographic needle electrode system (pO_2 histography) found average to high correlation, whereas no correlation was found with [^{18}F]-2-fluoro-2-deoxyglucose (FDG)[210]. A significant correlation was found between hypoxic tissue identified by FMISO and by immunohistochemical staining for both pimonidazole and carbonic anhydrase IX[220] (Dubois 2004).

Taken together, these imaging studies show that [^{18}F]FMISO is able to identify hypoxia, a unique feature of malignant and endangered tissues, thereby adding to the armamentarium of specific markers used to image tumors and potentially impact treatment for the benefit of individual patients. Low oxygenation status is often phenotypic of tumors that demonstrate a poor response to therapy, which justifies extensive investigation of the utility of agents like [^{18}F]FMISO to improve specific treatment regimens directed at hypoxic tumors.

The rationale for using a T:B ratio of 1.2 to separate normoxia from hypoxia is based on human and animal data. The initial animal results showed that normoxic myocardium

ratios were near unity over a wide range of flows. In numerous other organs of normal mice, rats, rabbits and dogs, the mean of the distribution histogram was 1.035, median 0.96, for 1342 samples[221]. Therefore, a cut-off of 1.2 was selected, with confidence that any T:B ratio above that value was indicative of hypoxic tissue. This conclusion is further justified by the human study presented in Figure 7. In this patient with a primary brain tumor, the FDG image was co-registered with the FMISO image (left panel). In brain regions far from the right frontal tumor, the T:B values for FMISO were uniformly less than 1.2, as depicted by the blue dots in the right panel, even though FDG SUV spanned a range from about 3 to 13. In the tumor area, a substantial fraction of the pixels were still in the normal range, but many values exceeded the cut-off as shown by the colored pixels in the FMISO image. A distribution histogram of the red data points shows a continuous distribution, reflecting the fact that the level of oxygenation is a continuum from normoxic to hypoxic. One consequence of this continuous scale is that FMISO images exhibit only modest contrast. However, the evidence that uptake is independent of blood flow and numerous other physiologic parameters, as described about, provides confidence that FMISO images uniquely identify tumors with prognostically significant levels of hypoxia.

FDG SUV

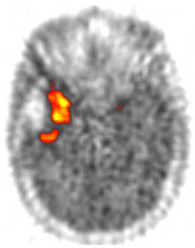

FMISO T: B

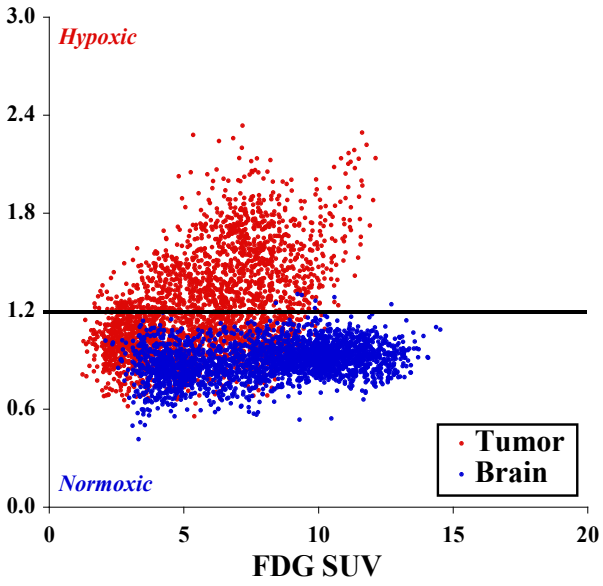

Figure 7. Right-frontal glioma post surgery.

VIII. REFERENCES

[1]. Prekeges JL, Rasey JS, Grunbaum Z, Krohn KH. Reduction of fluoromisonidazole, a new imaging agent for hypoxia. *Biochem Pharmacol.* 1991; 42 (12):2387-2395.

2. McClelland RA. Molecular interactions and biological effects of the products of reduction of nitroimidazoles. In*:* Adams GE, Breccia A, Fiedlen EN, and Wardoman P, eds. *NATO Advanced Research Workshop on Selective Activation of Drugs by Redox Processes*, New York, NY: Plenum Press, 1990.125-136.

3. Brown JM. Therapeutic targets in radiotherapy. *Int J Radiat Oncol Biol Phys* 2001; 49 (2):319-326.

4. Oswald J, Treite F, Haase C, et al. Experimental hypoxia is a potent stimulus for radiotracer uptake in vitro: Comparison of different tumor cells and primary endothelial cells. *Cancer Lett.* 2007; 254: 102-110.

5. Martin GV, Cerqueira MD, Caldwell JH, Rasey JS, Embree L, Krohn KA.. Fluoromisonidazole a metabolic marker of myocyte hypoxia. *Circ Res*. 1990; 67:240-244.

6. Rasey JS, Nelson NJ, Chin L, Evans ML, Grunbaum Z. Characteristics of the binding of labeled fluoromisonidazole in cells in vitro. *Radiat Res*. 1990; 122:301-308.

7. Rasey JS, Hoffman JM, Spence AM, Krohn KA. Hypoxia mediated binding of misonidazole in non-malignant tissue. *Int J Radiat Oncol Biol Phys*. 1986; 12:1255-1258.

8. Hoffman JM, Rasey JS, Spence AM, Shaw DW, Krohn KA. Binding of the hypoxia tracer [^{3}H]misonidazole in cerebral ischemia. *Stroke*. 1987; 18:168-176.

9. Piert M, Machulla HJ, Becker G, Aldinger P, Winter E, Bares R. Dependency of the [^{18}F]fluoromisonidazole uptake on oxygen delivery and tissue oxygenation in the porcine liver. *Nucl Med Biol.* 2000; 27:693-700.

10. Piert M, Machulla HJ, Becker G, et al. Introducing fluorine-18 fluoromisonidazole positron emission tomography for the localisation and quantification of pig liver hypoxia. *Eur J Nucl Med.* 1999; 26:95-109.

11. Smith BR, Born JL. Metabolism and excretion of [^{3}H]misonidazole by hypoxic rat liver. *Int J Radiat Oncol Biol Phys.* 1984; 10:1365-1370.

12. Riedl CC, Brader P, Zanzonico P, et al. Tumor hypoxia imaging in orthotopic liver tumors and peritoneal metastasis: A comparative study featuring dynamic ^{18}F-MISO and ^{124}I-IAZG PET in the same study cohort. *Eur J Nucl Med Mol Imaging.* 2008; 35:39-46.

13. Shelton ME, Dence CS, Hwang DR, Herrero P, Welch MJ, Bergmann SR. In vivo delineation of myocardial hypoxia during coronary occlusion using fluorine-18 fluoromisonidazole and positron emission tomography: a potential approach for identification of jeopardized myocardium. *J Am Coll Cardiol.* 1990; 16 (2):477-485.

14. Caldwell JH, Revenaugh JR, Martin GV, Johnson PM, Rasey JS, Krohn KA. Comparison of fluorine-18-fluorodeoxyglucose and tritiated fluoromisonidazole uptake during low-flow ischemia. *J Nucl Med*. 1995; 36:1633-1638.

15. Krohn KA, Link JM, Mason RP. Molecular Imaging of Hypoxia. *J Nucl Med*. 2008; 49:129S-148S.

16. Vallabhajosula S. ^{18}F-Labeled Positron Emission Tomographic Radiopharmaceuticals in Oncology: An overview of radiochemistry and mechanisms of tumor localization. *Semin Nucl Med.* 2007; 37:400-419.

17. Wiebe LI, Stypinski D. Pharmacokinetics of SPECT radiopharmaceuticals for imaging hypoxic tissues. *Q J Nucl Med*. 1996; 40:270-284

18. Chapman JD, Franko AJ, Sharplin J. A marker for hypoxic cells in tumours with potential clinical applicability. *Br J Cancer.* 1981; 43:546-550.

19. Nunn A, Linder K, Strauss HW. Nitroimidazoles and imaging hypoxia. *Eur J Nucl Med*. 1995; 22:265-280.

20. Franko AJ. Misonidazole and other hypoxia markers: Metabolism and applications. *Int J Radiat Oncol Biol Phys*. 1986; 12:1195-1202.

21. Wong KH, Wallen CA, Wheeler KT. Biodistribution of misonidazole and 1,3-bis(2-chloroethyl)-1-nitrosourea (BCNU) in rats bearing unclamped and clamped 9L subcutaneous tumors. *Int J Radiat Oncol Biol Phys*. 1989; 17:135-143.

22. Rajendran JG Krohn KA. Imaging hypoxia and angiogenesis in tumors. *Radiol Clin North Am*. 2005; 43:169-187.

23. Jerabek PA, Patrick TB, Kilbourn MR, Dischino DD, Welch MJ. Synthesis and biodistribution of ^{18}F-labeled fluoronitroimidazoles: Potential in vivo markers of hypoxic tissue. *Int J Rad Appl Instrum [A].* 1986; 37(7):599-605.

24. Grierson JR, Link JM, Mathis CA, Rasey JS, Krohn KA. Radiosynthesis of fluorine-18 fluoromisonidazole. *J Nucl Med*. 1989;30:343-350.

25. Grunbaum Z, Freauff SJ, Krohn KA, Wilbur DS, Magee S, Rasey JS. Synthesis and characterization of congeners of misonidazole for imaging hypoxia. *J Nucl Med*. 1987; 28:68-75.

26. Workman P. Pharmacokinetics of hypoxic cell radiosensitizers: a review. *Cancer Clin Trials*. 1980; 3:237-251.

27. Rasey JS, Grunbaum Z, Magee S, et al. Characterization of radiolabeled fluoromisonidazole as a probe for hypoxic cells. *Radiat Res*. 1987; 111:292-304.

28. Josephy PD, Mason RP. Nitroimidazoles. In*:* Anders M, (Ed), *Bioactivation of Foreign Compounds*, New York: Academic Press, 1985. p.451-483.

29. Flockhart IR, Sheldon PW, Stratford IJ, Watts ME. A metabolite of the 2-nitroimidazole misonidazole with radiosensitizing properties. *Int J Radiat Biol Relat Stud Phys Chem Med*. 1978a; 34(1):91-94.

30. Flockhart IR, Large P, Troup D, Malcolm SL, Marten TR. Pharmacokinetic and metabolic studies of the hypoxic cell radiosensitizer misonidazole. *Xenobiotica*. 1978b; 8(2):97-105.

31. Flockhart IR, Malcolm SL, Marten TR, Parkins CS, Ruane RJ, Troup D. Some aspects of the metabolism of misonidazole. *Br J Cancer Suppl III*. 1978c; 37:264-267.

32. Rasey JS, Koh W-J, Grierson JR, Grunbaum Z, and Krohn KA. Radiolabeled fluoromisonidazole as an imaging agent for tumor hypoxia. *Int J Radiat Oncol Biol Phys*. 1989; 17(5):985-991.

33. Moulder JE, Rockwell S. Hypoxic fractions of solid tumors: experimental techniques, methods of analysis, and a survey of existing data. *Int J Radiat Oncol Biol Phys*. 1984; 10:695-712.

[34]. Spence AM, Graham MM, Muzi M, et al. Deoxyglucose lumped constant estimated in a transplanted rat astrocytic glioma by the hexose utilization index. *J Cereb Blood Flow Metab*. 1990; 10:190-198.

35. Casciari JJ, Rasey JS. Determination of the radiobiologically hypoxic fraction in multicellular spheroids from data on the uptake of [^{3}H]fluoromisonidazole. *Radiat Res*. 1995; 141:28-36.

36. Koh W-J, Griffin TW, Rasey JS, Laramore GE. Positron emission tomography. A new tool for characterization of malignant disease and selection of therapy. *Acta Oncol*.1994; 33(3):323-327.

37. Whitmore GF, Gulyas S, Varghese AJ. Sensitizing and toxicity properties of misonidazole and its derivatives. *Br J Cancer*. 1978; 37(Suppl III):115-119.

38. Brown JM, Workman P. Partition coefficient as a guide to the development of radiosensitizers which are less toxic than misonidazole. *Radiat Res*. 1980; 82:171-190.

39. Stone HB, Sinesi MS. Testing of new hypoxic cell sensitizers in vivo. *Radiat Res*. 1982; 91: 186-198.

40. Graziano MJ, Henck JW, Meierhenry EF and Gough AW. Neurotoxicity of misonidazole in rats following intravenous administration. *Pharmacol Res.* 1996; 33(6): 307-318.

41. Dische S. Hypoxic cell sensitizers in radiotherapy. *Int J Radiat Oncol Biol Phys.* 1978; 4:157-160.

42. Phillips TL, Fu KK. The interaction of drug and radiation effects on normal tissues. *Int J Radiat Oncol Biol Phys*. 1978; 4:59-64.

43. Urtasun RC, Chapman JD, Feldstein ML, et al. Peripheral neuropathy related to misonidazole: Incidence and pathology. *Br J Cancer*. 1978; 37(Suppl III):271-275.

44. Overgaard J. Clinical evaluation of nitroimidazoles as modifiers of hypoxia in solid tumors. *Oncol Res*. 1994; 6:509-518.

45. Gray AJ, Dische S, Adams GE, Flockhart IR, Foster JL. Clinical testing of the radiosensitiser Ro-07-0582. I. Dose tolerance, serum and tumour concentrations. *Clin Radiol*. 1976; 27:151-157.

46. Saunders MI, Dische S, Anderson P, and Flockhart IR. The neurotoxicity of misonidazole and its relationship to dose, half-life and concentration in the serum. *Br J Cancer*.1978; 37(Suppl III):268-270.

47. Wasserman TH, Phillips TL, Johnson RJ, et al. Initial united states clinical and pharmacologic evaluation of misonidazole (Ro-07-0582), an hypoxic cell radiosensitizer. *Int J Radiat Oncol Biol Phys*. 1979; 5:775-786.

48. Wiltshire CR, Workman P, Watson JV, and Bleehen NM. Clinical studies with misonidazole. *Br J Cancer.* 1978; 37(Suppl III):286-9.

[49]. Dische S. Misonidazole in the clinic at Mount Vernon. *Cancer Clin Trials*. 1980; 3:175-178.

50. Dische S, Saunders MI, Flockhart IR, Lee ME, Anderson P. Misonidazole-a drug for trial in radiotherapy and oncology. *Int J Radiat Oncol Biol Phys*. 1979; 5:851-860.

51. Paget GE. Toxicity tests: A guide for clinicians. *J New Drugs*. 1962; 2(2):78-83.

52. Rasey JS, Martin, GV, Krohn, KA. Quantifying hypoxia with radiolabeled fluoromisonidazole: Pre-clinical and clinical studies. In*:* Machulla HJ, ed. *Imaging of Hypoxia: Tracer Developments*. Dordrecht, The Netherlands: Kluwer Academic Publishers,;1999:85-117.

53. Koh W-J, Bergman KS, Rasey JS, et al. Evaluation of oxygenation status during fractionated radiotherapy in human nonsmall cell lung cancers using [F-18]fluoromisonidazole positron emission tomography. *Int J Radiat Oncol Biol Phys*. 1995; 33(2):391-398.

54. Rajendran JG, Mankoff DA, O'Sullivan F, et al. Hypoxia and glucose metabolism in malignant tumors: evaluation by [^{18}F]fluoromisonidazole and [^{18}F]fluorodeoxyglucose positron emission tomography imaging. *Clin Cancer Res*. 2004; 10:2245-2252.

55. Graham MM, Peterson LM, Link JM, et al. Fluorine-18-fluoromisonidazole radiation dosimetry in imaging studies. *J Nucl Med*. 1997; 38(10):1631-1636.

56. Silverman DHS, Hoh CK, Seltzer MA, et al. Evaluating tumor biology and oncological disease with positron-emission tomography. *Semin Radiat Oncol*. 1998; 8(3):183-196.

57. Rofstad EK, Danielsen T. Hypoxia-induced metastasis of human melanoma cells: involvement of vascular endothelial growth factor-mediated angiogenesis. *Br J Cancer.* 1999; 80:1697-1707.

58. Rischin D, Peters L, Hicks R, et al. Phase I trial of concurrent tirapazamine, cisplatin, and radiotherapy in patients with advanced head and neck cancer. *J Clin Oncol.* 2001; 19(2):535-542.

59. Valk PE, Mathis CA, Prados MD, Gilbert JC, and Budinger TF. Hypoxia in human gliomas: Demonstration by PET with fluorine-18-fluoromisonidazole. *J Nucl Med*. 1992; 33:2133-2137.

60. Eschmann S-M, Paulsen F, Reimold M, et al. Prognostic impact of hypoxia imaging with ^{18}f-misonidazole PET in non-small cell lung cancer and head and neck cancer before radiotherapy. *J Nucl Med*. 2005; 46:253-260.

61. Read SJ, Hirano T, Abbott DF, et al. Identifying hypoxic tissue after acute ischemic stroke using PET and ^{18}F-fluoromisonidazole. *Neurology*. 1998; 51(6):1617-1621.

62. Miller RC, Hall EJ. Oncogenic transformations in vitro produced by misonidazole. *Cancer Clin Trials*. 1980; 3:85-90.

63. Chin JB, Sheinin DMK, Rauth AM. Screening for the mutagenicity of nitro-group containing hypoxic cell radiosensitizers using salmonella typhimurium strains TA 100 and TA 98. *Mutat Res*. 1978; 58:1-10.

64. Suzanger M, White INH, Jenkins TC, Connors TA. Effects of substituted 2-nitromisonidazoles and related compounds on unscheduled DNA synthesis in rat hepatocytes and in non-transformed (BL8) and transformed (JB1) rat liver epithelial derived cell lines. *Biochem Pharmacol*. 1987; 36(21): 3743-3749.

[65]. Mortensen, LS; Buus, S; Nordsmark, M; Bentzen, L; Munk, OL; Keiding, S; Overgaard, J. Identifying Hypoxia in Human Tumors: A Correlation Study between 18 F-FMISO PET and the Eppendorf Oxygen-Sensitive Electrode. Acta Oncologica, 2010; 49: 934–940

[66] Yoon J, Kang S, Lee K, et al. Targeting Hypoxia Using Evofosfamide and Companion Hypoxia Imaging of FMISO-PET in Advanced Biliary Tract Cancer. Cancer Res Treat. 2021; 53(2):471-479.

[67] Rogasch J, Beck M, Stromberger C, et al. PET measured hypoxia and MRI parameters in re-irradiated head and neck squamous cell carcinomas: findings of a prospective pilot study [version 1; peer review: 1 approved, 1 approved with reservations]. Mathematical Biosciences and Engineering. 2021.

[68] Thureau S, Piton N, Gouel P, et al. First Comparison between [18f]-FMISO and [18f]-Faza for Preoperative Pet Imaging of Hypoxia in Lung Cancer. Cancers. August 14, 2021.

[69] Suzuki K, Kawai N, Ogawa T, et al. Hypoxia and glucose metabolism assessed by FMISO and FDG PET for predicting IDH1 mutation and 1p/19q codeletion status in newly diagnosed malignant gliomas. EJNMMI Research. 2021; 11:67.

[70] Rühle A, Grosu A, Wiedenmann N, et al. Immunohistochemistry-based hypoxia-immune prognostic classifier for head-and-neck cancer patients undergoing chemoradiation – Post-hoc analysis from a prospective imaging trial. Radiotherapy and Oncology. 2021; 159:75-81.

[71] Paudya R, Grkovski M, Oh J, et al. Application of Community Detection Algorithm to Investigate the Correlation between Imaging Biomarkers of Tumor Metabolism,

Hypoxia, Cellularity, and Perfusion for Precision Radiotherapy in Head and Neck Squamous Cell Carcinomas. Cancers. August 3, 2021.

[72] Nehmeh S, Moussa M, Lee N, et al. Comparison of FDG and FMISO uptakes and distributions in head and neck squamous cell cancer tumors. EJNMMI Research. 2021; 11:(38).

[73] López-Vega J, Álvarez I, Anton A, et al. Early Imaging and Molecular Changes with Neoadjuvant Bevacizumab in Stage II/III Breast Cancer. Cancers. July 14, 2021.

[74] Lee S, Tebbutt N, Gan H, et al. Evaluation of ^{18}F-FMISO PET and ^{18}F-FDG PET Scans in Assessing the Therapeutic Response of patients with metastatic Colorectal Cancer Treated with Anti-Angiogenic Therapy. Frontier in Oncology. March 17, 2021; 11.

[75] Lee S, Muralidharan V, Tebbut N, et al. Prevalence of hypoxia and correlation with glycolytic metabolism and angiogenic biomarkers in metastatic colorectal carcinoma. European Journal of Nuclear Medicine and Molecular Imaging. 2021; 48.

[76] Lazzeroni M, Ureba A, Wiedenmann N, et al. Evolution of the hypoxic compartment on sequential oxygen partial pressure maps during radiochemotherapy in advanced head and neck cancer. Physics and Imaging in Radiation Oncology. 2021; 17:100-105.

[77] Huang S, Michalek J, Reardon D, et al. Assessment of tumor hypoxia and perfusion in recurrent glioblastoma following bevacizumab failure using MRI and ^{18}F-FMISO PET. Scientific reports. 2021; 11:7632.

[78] Collet S, Guillamo J, Berro D, et al. Simultaneous Mapping of Vasculature, Hypoxia, and Proliferation Using Dynamic Susceptibility Contrast MRI, ^{18}F-FMISO PET, and ^{18}F-FLT PET in Relation to Contrast Enhancement in Newly Diagnosed Glioblastoma. Journal of Nuclear Medicine. 2021; 62:1349–1356.

[79] Carmona-Bozo J, Manavaki R, Woitek R, et al. Hypoxia and perfusion in breast cancer: simultaneous assessment using PET/MR imaging. European Radiology. 2021; 31:333-344.

[80] Zschaeck S, Zöphel K, Seidlitz A, et al. Generation of biological hypotheses by functional imaging links tumor hypoxia to radiation induced tissue inflammation/glucose uptake in head and neck cancer. Radiotherapy and Oncology. 2021; 155:204-211.

[81] Carles M, Fechter T, Grosu A, et al. ^{18}F-FMISO-PET Hypoxia Monitoring for Head-and-Neck Cancer Patients: Radiomics Analyses Predict the Outcome of Chemo-Radiotherapy. Cancers. July 9, 2021.

[82] Socarrás Fernándeza J, Mönnich D, Leibfarth S, et al. Comparison of patient stratification by computed tomography radiomics and hypoxia positron emission tomography in head-and-neck cancer radiotherapy. Physics and Imaging in Radiation Oncology. 2020; 15:52-59.

[83] Leimgruber A, Hickson K, Lee S, et al. Spatial and quantitative mapping of glycolysis and hypoxia in glioblastoma as a predictor of radiotherapy response and sites of relapse. European Journal of Nuclear Medicine and Molecular Imaging. 2020; 47:1476–1485.

[84] Nicolay N, Wiedenmann N, Mix M, et al. Correlative analyses between tissue-based hypoxia biomarkers and hypoxia PET imaging in head and neck cancer patients during radiochemotherapy—results from a prospective trial. European Journal of Nuclear Medicine and Molecular Imaging. 2020; 47:1046–1055.

[85] Rühle A, Grosu A, Wiedenmann N, et al. Hypoxia dynamics on FMISO-PET in combination with PD-1/PD-L1 expression has an impact on the clinical outcome of patients with Head-and-neck Squamous Cell Carcinoma undergoing Chemoradiation. Theranostics. 2020; 10: 20.

[86] Shima T, Fujima N, Yamano S, et al. Evaluation of non-Gaussian model-based diffusion-weighted imaging in oral squamous cell carcinoma: Comparison with tumour functional information derived from positronemission tomography. Clinical Radiology. 2020; 75:397.e15e397.e21.

[87] Sörensen A, Carles M, Bunea H, et al. Textural features of hypoxia PET predict survival in head and neck cancer during chemoradiotherapy. European Journal of Nuclear Medicine and Molecular Imaging. 2020; 47:1056–1064.

[88] Thureau S, Modzelewski R, Bohn P, et al. Comparison of Hypermetabolic and Hypoxic Volumes Delineated on [^{18}F]FDG and [^{18}F]Fluoromisonidazole PET/CT in Non-small-cell Lung Cancer Patients. Mol Imaging Biol. 2020; 22:764-771.

[89] Wiedenmann N, Grosu A, Buchert M, et al. The utility of multiparametric MRI to characterize hypoxic tumor subvolumes in comparison to FMISO PET/CT. Consequences for diagnosis and chemoradiation treatment planning in head and neck cancer. Radiotherapy and Oncology. 2020; 150:128–135.

[90] Zschaeck S, Lock S, Hofheinz F, et al. Individual patient data meta-analysis of FMISO and FAZA hypoxia PET scans from head and neck cancer patients undergoing definitive radiochemotherapy. Radiotherapy and Oncology. 2020; 149:189–196.

[91] Andrzejewski P, Wengert G, Helbich T, et al. Sequential [^{18}F]FDG-[^{18}F]FMISO PET and Multiparametric MRI at 3T for Insights into Breast Cancer Heterogeneity and Correlation with Patient Outcomes: First Clinical Experience. Hindawi. 2019.

[92] Bandurska-Luque A, Löck S, Haase R, et al. FMISO-PET-based lymph node hypoxia adds to the prognostic value of tumor only hypoxia in HNSCC patients. Radiotherapy and Oncology. 2019; 130:97–103.

[93] Cegla P, Joanna K, Sebastian G, et al. Correlation between tumour biology status measured in triple-tracer ^{18}F-fluorodeoxyglucose–^{18}F-fluorothymidine–^{18}F-fluoromisonidazole-PET/CT study and human papillomavirus status in patients with head and neck cancer. Nuclear Medicine Communication. 2019; 40:752–757.

[94] Jagtap R, Asopa R, Basu S. Evaluating cardiac hypoxia in hibernating myocardium: Comparison of 9mTc-MIBI/^{18}F-fluorodeoxyglucose and ^{18}F-fluoromisonidazole positron emission tomography-computed tomography in relation to normal, hibernating, and infarct myocardium. World Journal of Nuclear Medicine. 2019.

[95] Kroenke M, Hirata K, Gafita A, et al. Voxel based comparison and texture analysis of 18F-FDG and 18F-FMISO PET of patients with head-and-neck cancer. PLOSONE. February 28, 2019.

[96] Löck S, Linge A, Seidlitz A, at al. Repeat FMISO-PET imaging weakly correlates with hypoxia-associated gene expressions for locally advanced HNSCC treated by primary Radiochemotherapy. Radiotherapy and Oncology. 2019; 135:43–50.

[97] McGowan D, Skwarski M, Bradley K, et al. Buparlisib with thoracic radiotherapy and its effect on tumour hypoxia: A phase I study in patients with advanced non-small cell lung carcinoma. European Journal of Cancer. 2019; 113:87-95.

[98] Shimizu Y, Kudo K, Kameda H, et al. Prediction of Hypoxia in Brain Tumors Using a Multivariate Model Built from MR Imaging and ^{18}F-Fluorodeoxyglucose Accumulation Data. Magnetic Resonance in Medical Sciences. 2020; 19(13):227–234.

[99] Supiot S, Rousseau C, Dore M, et al. Reoxygenation during radiotherapy in intermediate-risk prostate cancer. Radiotherapy and Oncology. 2019; 133:16–19.

[100] Thorwarth D, Welz Stefan, Monnich D, et al. Prospective Evaluation of a Tumor Control Probability Model Based on Dynamic ^{18}F-FMISO PET for Head and Neck Cancer Radiotherapy. Journal Nuclear Medicine. 2019; 60:1698–1704.

[101] Vera P, Mihailescu S, Lequesne J, et al. Radiotherapy boost in patients with hypoxic lesions identified by ^{18}F-FMISO PET/CT in non-small-cell lung carcinoma: can we expect a better survival outcome without toxicity? [RTEP5 long-term follow-up]. European Journal of Nuclear Medicine and Molecular Imaging. 2019; 46:1448–1456.

[102] Watanabe S, Inoue T, Okamoto S, et al. Combination of FDG-PET and FMISO-PET as a treatment strategy for patients undergoing early-stage NSCLC stereotactic radiotherapy. EJNMMI Research. 2019; 9:104.

[103] Yamane T, Aikawa M, Yasuda M, et al. [^{18}F]FMISO PET/CT as a preoperative prognostic factor in patients with pancreatic cancer. EJNMMI Research. 2019; 9:39.

[104] Abdo R, Lamare F, Fernandez P, and Bentourkia M. Analysis of hypoxia in human glioblastoma tumors with dynamic ^{18}F-FMISO PET imaging. Australasian Physical & Engineering Sciences in Medicine. 2019; 42:981–993.

[105] Kobayashi K, Manabe O, Hirata K, et al. Influence of the scan time point when assessing hypoxia in ^{18}F-fluoromisonidazole PET: 2 vs. 4 h. European Journal of Nuclear Medicine and Molecular Imaging. 2020; 47:1833–1842.

[106] Li H, Xu D, Han X, et al. Dosimetry study of ^{18}F-FMISO + PET/CT hypoxia imaging guidance on intensity-modulated radiation therapy for non-small cell lung cancer. Clinical and Translational Oncology. 2018; 20:1329–1336.

[107] Li L, Wei Y, Huang Y, et al. To Explore a Representative Hypoxic Parameter to Predict the Treatment Response and Prognosis Obtained by [^{18}F]FMISO-PET in Patients with Non-small Cell Lung Cancer. Molecular Imaging Biology. 2018; 20:1061-1067.

[108] Thureau S, Dubray B, Modzelewski R, et al. FDG and FMISO PET-guided dose escalation with intensity-modulated radiotherapy in lung cancer. Radiation Oncology. 2018; 13:208.

[109]. Wiedenmann N, Bunea H, Rischke H, et al. Effect of radiochemotherapy on T2* MRI in HNSCC and its relation to FMISO PET derived hypoxia and FDG PET. Wiedenmann et al. Radiation Oncology. 2018; 13:159.

[110]. Tachibana I, Nishimura Y, Hanaoka K, et al. Tumor Hypoxia Detected by 18F-fluoromisonidazole Positron Emission Tomography (FMISO PET) as a Prognostic Indicator of Radiotherapy (RT). Anticancer Research. 2018; *38*: 1775-1781.

[111]. Supiot S, Rousseau C, Dore M, et al. Evaluation of tumor hypoxia prior to radiotherapy in intermediate-risk prostate cancer using ^{18}F-fluoromisonidazole PET/CT: a pilot study. Oncotarget. 2018; 9(11).

[112]. Sato J, Kitagawa Y, Watanabe S, et al. Hypoxic volume evaluated by 18F-fluoromisonidazole positron emission tomography (FMISO-PET) may be a prognostic factor in patients with oral squamous cell carcinoma: preliminary analyses. Int. J Oral Maxillofac Surg. 2018; 47: 553–560.

[113]. Ratai E, Zhang Z, Fink James, et al. ACRIN 6684: Multicenter, phase II assessment of tumor hypoxia in newly diagnosed glioblastoma using magnetic resonance spectroscopy. PLOS ONE. June 14, 2018.

[114]. Nehmeh S. Schwartz J, Grkovski M, et al. Inter-operator variability in compartmental kinetic analysis of 18F-fluoromisonidazole dynamic PET. Clin Imaging. 2018; 49: 121–127.

[115]. McGowan D, Skwarski M, Papiez B, et al. Whole tumor kinetics analysis of 18Ffluoromisonidazole dynamic PET scans of non-small cell lung cancer patients, and correlations with perfusion CT blood flow. McGowan et al. EJNMMI Research (2018) 8:73.

[116]. Li L, Wei Y, Huang Y, et al. To Explore a Representative Hypoxic Parameter to Predict the Treatment Response and Prognosis Obtained by [18F]FMISO-PET in Patients with Non-Small Cell Lung Cancer. Mol Imaging Biol. 2018.

[117]. Li H, Xu D, Han X, et al. Dosimetry study of 18F-FMISO + PET/CT hypoxia imaging guidance on intensity-modulated radiation therapy for non-small cell lung cancer. Clinical and Translational Oncology (2018) 20:1329–1336.

[118]. Crispin-Ortuzar M, Apte A, Grkovski M, et al. Predicting hypoxia status using a combination of contrast-enhanced computed tomography and [18F]-Fluorodeoxyglucose positron emission tomography radiomics features. Radiotherapy and Oncology 127 (2018) 36–42.

[119]. Chatterjee A, Gupta T, Rangarajan V, et al. Optimal timing of fluorine-18-fluoromisonidazole positron emission tomography/computed tomography for assessment of tumor hypoxia in patients with head and neck squamous cell carcinoma. Nuclear Medicine Communications 2018, 39:859–864.

[120]. Asano A, Ueda S, Kuji I, et al. Intracellular hypoxia measured by 18F-fluoromisonidazole positron emission tomography has prognostic impact in patients with estrogen receptor-positive breast cancer. Breast Cancer Research. (2018) 20:78.

[121]. Schwartz J, Grkovski M, Rimner A, et al. Pharmacokinetic Analysis of Dynamic ^{18}F-Fluoromisonidazole PET Data in Non–Small Cell Lung Cancer. J Nucl Med. 2017; 58:911–919.

[122]. Welz S, Monnich D, Pfannenberg C, et al. Prognostic value of dynamic hypoxia PET in head and neck cancer: Results from a planned interim analysis of a randomized phase II hypoxia-image guided dose escalation trial. Radiotherapy and Oncology. 2017; 124: 526-532.

[123]. Ueda S, Saeki T, Osaki A, et al. Bevacizumab Induces Acute Hypoxia and Cancer Progression in Patients with Refractory Breast Cancer: Multimodal Functional Imaging and Multiplex Cytokine Analysis. Clin Cancer Res. July 5, 2017. [Epub ahead of print].

[124]. Toyonaga T, Yamaguchi S, Hirata K, et al. Hypoxic glucose metabolism in glioblastoma as a potential prognostic factor. Eur J Nucl Med Mol Imaging. 2017; 44: 611–619.

[125]. Simoncic U, Leibfarth S, Schmidt N, et al. Comparison of DCE-MRI kinetic parameters and FMISO-PET uptake parameters in head and neck cancer patients. Med. Phys. June 2017; 44 (6).

[126]. Sato J, Kitagawa Y, Watanabe S, et al. ^{18}F-Fluoromisonidazole positron emission tomography (FMISO-PET) may reflect hypoxia and cell proliferation activity in oral squamous cell carcinoma. Oral and Maxillofacial Pathology. September 2017; 124:3.

[127]. Qiu J, Lv B, Fu M, et al. ^{18}F-Fluoromisonidazole positron emission tomography/CT-guided volumetric-modulated arc therapy-based dose escalation for hypoxic subvolume in nasopharyngeal carcinomas: A feasibility study. Head & Neck. 2017; 39:2519–2527.

[128]. Puri T, Greenhalgh T, Wilson J, et al. [^{18}F]Fluoromisonidazole PET in rectal Cancer. EJNMMI Research. 2017; 7:78.

[129]. Preibisch C, Shi K, Kluge A, et al. Characterizing hypoxia in human glioma: A simultaneous multimodal MRI and PET study. NMR in Biomedicine. 2017; 30: e3775.

[130]. Nishikawa Y, Yasuda K, Okamoto S, et al. Local relapse of nasopharyngeal cancer and Voxel-based analysis of FMISO uptake using PET with semiconductor detectors. Radiation Oncology. 2017; 12:148.

[131]. Mönnich D, Thorwarth D, Leibfarth S, et al. Overlap of highly FDG-avid and FMISO hypoxic tumor subvolumes in patients with head and neck cancer. ACTA ONCOLOGICA. 2017; VOL. 56, NO. 11, 1577–1582.

[132]. McGowan D, Macpherson R, Hackett S, et al. ^{18}F-fluoromisonidazole uptake in advanced stage non-small cell lung cancer: A voxel-by-voxel PET kinetics study. Med. Phys. 2017; 44 (9).

[133]. Löck S, Perrin R, Seidlitz A, et al. Residual tumour hypoxia in head-and-neck cancer patients undergoing primary radiochemotherapy, final results of a prospective trial on repeat FMISO-PET imaging. Radiotherapy and Oncology. 2017; 124: 533-540.

[134]. Kelada O, Decker R, Nath S, et al. High Single Doses of Radiation May Induce Elevated Levels of Hypoxia in Early-Stage Non-Small Cell Lung Cancer Tumors. Int J Radiation Oncol Biol Phys, Vol. 102, No. 1, pp. 174e183, 2017.

[135]. Kanoto M, Kirii K, Hiraka T, et al. Correlation between hypoxic area in primary brain tumors and WHO grade: differentiation from malignancy using ^{18}F-fluoromisonidazole positron emission tomography. Acta Radiologica. 2017; 0(0) 1–7.

[136]. Grkovski M, Schöder H, Lee N, et al. Multiparametric Imaging of Tumor Hypoxia and Perfusion with ^{18}F-Fluoromisonidazole Dynamic PET in Head and Neck Cancer. J Nucl Med. 2017; 58: 1072–1080.

[137]. Grkovski M, Lee N, Schöder H, et al. Monitoring early response to chemoradiotherapy with ^{18}F-FMISO dynamic PET in head and neck cancer. Eur J Nucl Med Mol Imaging. 2017; 44: 1682–1691.

[138]. Georg P, Andrzejewski P, Baltzer P, et al. Changes in Tumor Biology During Chemoradiation of Cervix Cancer Assessed by Multiparametric MRI and Hypoxia PET. Mol Imaging Biol. 2017.

[139]. Daniel M, Andrzejewski P, Sturdza A, et al. Impact of hybrid PET/MR technology on multiparametric imaging and treatment response assessment of cervix cancer. Radiotherapy and Oncology 125 (2017) 420–425.

[140]. da Ponte K, Berro D, Collet S, et al. In Vivo Relationship Between Hypoxia and Angiogenesis in Human Glioblastoma: A Multimodal Imaging Study. J Nucl Med 2017; 58:1574–1579.

[141]. Chakhoyan A, Guillamo J, Collet S, et al. FMISO-PET-derived brain oxygen tension maps: application to glioblastoma and less aggressive gliomas. Sci Report. August 31, 2017 [Epub ahead of print].

[142]. Boeke S, Thorwarth D, Mönnich D, et al. Geometric analysis of loco-regional recurrences in relation to pre-treatment hypoxia in patients with head and neck cancer. ACTA ONCOLOGICA, 2017; 56: 11, 1571–1576.

[143]. Bekaert L, Valable S, Lechapt-Zalcman, E, et al. [^{18}F]-FMISO PET study of hypoxia in gliomas before surgery: correlation with molecular markers of hypoxia and angiogenesis. Eur J Nucl Med Mol Imaging. 2017; 44: 1383–1392.

[144]. Wei Y, Zhao W, Huang Y, et al. A Comparative Study of Noninvasive Hypoxia Imaging with 18F-Fluoroerythronitroimidazole and ^{18}F-Fluoromisonidazole PET/CT in Patients with Lung Cancer. Plos One. June 20, 2016.

[145]. Quintela-Fandino M, Lluch A, Manso LM, et al. ^{18}F-fluoromisonidazole PET and activity of neoadjuvant nintedanib in early HER2-negative breast cancer: a window-of-opportunity randomized trial. Clinical Cancer Resources. September 2016: [Epub ahead of print].

[146]. Lee N, Schoder H, Beattie B, et al. Strategy of Using Intratreatment Hypoxia Imaging to Selectively and Safely Guide Radiation Dose De-escalation Concurrent with Chemotherapy for Locoregionally Advanced Human Papillomaviruse-Related Oropharyngeal Carcinoma. Radiation Oncology Int J Oncol boil phys. April 2016. 96: 1, 9-17.

[147]. Grkovski M, Schwartz J, Rimner A, et al. Reproducibility of ^{18}F-fluoromisonidazole intratumour distribution in non-small cell lung cancer. EJNMMI Research. (2016); 6:79.

[148]. Bittner M, Wiedenmann N, Bucher S, et al. Analysis of relation between hypoxia PET imaging and tissue-based biomarkers during head and neck radiochemotherapy. ACTA ONCOLOGICA, 2016; 55: 11, 1299–1304.

[149]. Barajas Jr. R, Krohn K, Link J, et al. Glioma FMISO PET/MR Imaging Concurrent with Antiangiogenic Therapy: Molecular Imaging as a Clinical Tool in the Burgeoning Era of Personalized Medicine. Biomedicines. 2016; 4: 24.

[150]. Zheng M, Collier L, Bois F, et al. Synthesis of [^{18}F]FMISO in a Flow-Through Microfluidic Reactor: Development and Clinical Application. Nucl Med and Biol. 2015; 42: 578-584.

[151]. Sachpekidis, C, Thieke C, Askoxylakis V, et al. Combined use of ^{18}F-FDG and ^{18}F-FMISO in Unresectable Non-Small Cell Lung Cancer Patients Planned for Radiotherapy: A Dynamic PET/CT Study. Am J Nucl Med Mol Imaging. 2015; 5(2):127-142.

[152]. Barajas Jr. R, Pampaloni M, Clarke J, et al. Assessing Biological Response to Bevacizumab Using ^{18}F-Fluoromisonidazole PET/MR Imaging in a Patient with Recurrent Anaplastic Astrocytoma. Hindawi. February 2015.

[153]. Arvold N, Heidari P, Kunawudhi A, et al. Tumor Hypoxia Response After Targeted Therapy in EGFR-Mutant Non-Small Cell Lung Cancer: Proof of Concept for FMISO-PET. Technology in Cancer Research & Treatment. January 2015.

[154]. Ueda, S, Kuji I, Shigekawa T, et al. Optical Imaging for Monitoring Tumor Oxygenation Response after Initiation of Single-Agent Bevacizumab followed by Cytotoxic Chemotherapy in Breast Cancer Patients. PLoS ONE. 2014; 9(6).

[155]. Sato J, Kitagawa Y, Yamazaki Y, et al. Advantage of FMISO-PET over FDG-PET for predicting histological response to preoperative chemotherapy in patients with oral squamous cell carcinoma. Eur J Nucl Med Mol Imaging. 2014; 41:2031–2041.

[156]. Rockne R, Trister A, Jacobs J, et al. A Patient-Specific Computational Model of Hypoxia-Modulated Radiation Resistance in Glioblastoma Using ^{18}F-FMISO-PET. The Royal Society Publishing. December 2014.

[157]. Lee G, Kim J, Oh S, Kang D, Kim J, Kwon S. ^{18}F-fluoromisonidazole (FMISO) Positron Emission Tomography (PET) Predicts Early Infarct Growth in Patients with Acute Ischemic Stroke. J Neuroimaging. 2014; 1-4.

[158]. de Figueiredo B, Zacharatou C, Galland-Girodet S, et al. Hypoxia imaging with [18F]-FMISO-PET for guided dose escalation with intensity-modulated radiotherapy in head-andneck cancers. Strahlenther Onkol. Epub Sept 23, 2014.

[159]. Thureau S, Chaumet-Riffaud P, Modzelewski R, et al. Interobserver Agreement of Qualitative Analysis and Tumor Delineation of ^{18}F-Fluoromisonidazole and 39-Deoxy-39-^{18}F-Fluorothymidine PET Images in Lung Cancer. J Nucl Med. 2013; 54:1543–1550. Epub Aug 5, 20

[160]. Tachibana I, Nishimura Y, Shibata T, et al. A prospective clinical trial of tumor hypoxia imaging with ^{18}F-fluoromisonidazole positron emission tomography and computed tomography (F-MISO PET/CT) before and during radiation therapy. J Rad Res. 2013; 54, 1078–1084. Epub Mar 22, 2013.

[161]. Segard T, Robins P, Yusoff Ian, et al. Detection of Hypoxia With ^{18}F-Fluoromisonidazole (^{18}F-FMISO) PET/CT in Suspected or Proven Pancreatic Cancer. Clin Nucl Med. 2013;38: 1-6. Epub Aug 22, 2012.

[162]. Sato J, Kitagawa Y, Yamazaki Y, et al. ^{18}F-Fluoromisonidazole PET Uptake Is Correlated with Hypoxia-Inducible Factor-1a Expression in Oral Squamous Cell Carcinoma. J Nucl Med. 2013; 54:1060–1065. Epub May 22, 2013.

[163]. Okamoto S, Shiga T, Yasuda K, et al. High Reproducibility of Tumor Hypoxia Evaluated by ^{18}F-Fluoromisonidazole PET for Head and Neck Cancer. J Nucl Med. 2013; 54:201–207. Epub Jan 15, 2013.

[164]. Norikane T, Yamamoto Y, Maeda Y, et al. Correlation of ^{18}F-fluoromisonidazole PET findings with HIF-1a and p53 expressions in head and neck cancer: comparison with ^{18}F-FDG PET. Nucl Med Commun. Epub Oct 10, 2013.

[165]. de Figueiredo B, Merlin T, de Clermont-Gallerande, H, et al. Potential of [^{18}F]-Fluoromisonidazole positron-emission tomography for radiotherapy planning in head and neck squamous cell carcinomas. Strahlenther Onkol. 2013; 189:1015–1019. Epub Aug 5, 2013.

[166]. Chang J, Wada M, Anderson, N, et al. Hypoxia-targeted radiotherapy dose painting for head and neck cancer using ^{18}F-FMISO PET: A biological modeling study. Acta Oncologica. 2013; 52: 1723–1729. Epub Dec 11, 2012.

[167]. Bittner M, Wiedenmann N, Bucher S, et al. Exploratory geographical analysis of hypoxic subvolumes using 18F-MISO-PET imaging in patients with head and neck cancer in the course of primary chemoradiotherapy. Radiotherapy and Oncology. 2013; (108):511–516.

[168]. Alawneh J, Moustafa R, Marrapu S, et al. Diffusion and perfusion correlates of the ^{18}F-MISO PET lesion in acute stroke: pilot study. Eur J Nucl Med Mol Imaging. Epub Oct 15.

[169]. Narita T, Aoyama H, Hirata K, et al. Reoxygenation of glioblastoma multiforme treated with fractionated radiotherapy concomitant with temozolomide: changes defined by 18F fluoromisonidazole positron emission tomography: two case reports. Jpn J Clin Oncol, 2012;42(2):120-3. Epub Dec 23, 2011.

[170]. Toma-Dasu I, Uhrdin J, Antonovic L, et al. Dose prescription and treatment planning based on FMISO-PET hypoxia. Acta Oncol, 2012;51(2):222-30. Epub Aug 28, 2011.

[171]. Hirata K, Terasaka S, Shiga T, Et Al. ^{18}F-Fluoromisonidazole positron emission tomography may differentiate glioblastoma multiforme from less malignant gliomas. Eur J Nucl Med Mol Imaging, 2012;39(5):760-70. Epub Feb 4, 2012.

[172]. Yamamoto Y, Maeda Y, Kawai N, et al. Hypoxia assessed by 18F-fluoromisonidazole positron emission tomography in newly diagnosed gliomas. Nucl Med Commun, 2012;33(6):621-5.

[173]. Mammar H, Kerrou K, Nataf V, Et Al. Positron Emission tomography/computed tomography imaging of residual skull base chordoma before radiotherapy using fluoromisonidazole and fluorodeoxyglucose: Potential consequences for dose painting. Int J Radiat Oncol Biol Phys, 2012;84(3):681-7. Epub Mar 3, 2012.

[174]. Yasuda K, Onimaru R, Okamoto S, et al. [18F]fluoromisonidazole and a new PET system with semiconductor detectors and a depth of interaction system for intensity modulated radiation therapy for nasopharyngeal cancer. Int J Radiat Oncol Biol Phys, 2012 May 12.

[175]. Chen L, Zhang Z, Kolb Hc, Walsh Jc, Zhang J, Guan Y. ^{18}F-Hx4 hypoxia imaging with PET/CT in head and neck cancer: A comparison with ^{18}F-Fmiso. Nucl Med Commun, 2012;33(10):1096-102.

[176]. Zips D, Zöphel K, Abolmaali N, et al. Exploratory prospective trial of hypoxia-specific PET imaging during radiochemotherapy in patients with locally advanced head-and-neck cancer. Radiotherp Oncol, 2012;105(1):21-8. Epub Sep 27, 2012.

[177]. Mckeage Mj, Jameson Mb, Ramanathan Rk, Et Al. Pr-104 A bioreductive pre-prodrug combined with gemcitabine or docetaxel in a phase Ib study of patients with advanced solid tumours. Bmc Cancer, 2012;12:496.

[178]. Kawai N, Maeda Y, Kudomi N, et al. Correlation of biological aggressiveness assessed by 11C-methionine PET and hypoxic burden assessed by 18F-fluoromisonidazole PET in newly diagnosed glioblastoma. Eur J Nucl Med Mol Imaging, 2011;38(3):441-50. Epub Nov 12, 2010.

[179]. Vera P, Bohn P, Edet-Sanson A, et al. Simultaneous positron emission tomography (PET) assessment of metabolism with ^{18}F-fluoro-2-deoxy-d-glucose (FDG), proliferation with ^{18}F-fluoro-thymidine (FLT), and hypoxia with ^{18}fluoro-misonidazole (F-miso) before and during radiotherapy in patients with non-small-cell lung cancer (NSCLC): a pilot study. Radiother Oncol, 2011;98(1):109-16. Epub Nov 4, 2010.

[180]. Eary Jf, Link Jm, Muzi M, Et Al. Multiagent pet for risk characterization in sarcoma. J Nucl Med, 2011;52(4):541-6. Epub Mar 18, 2011.

[181]. Kikuchi M, Yamane T, Shinohara S, et al. 18F-fluoromisonidazole positron emission tomography before treatment is a predictor of radiotherapy outcome and survival prognosis in patients with head and neck squamous cell carcinoma. Ann Nucl Med, 2011;25(9):625-33. Epub Jul 1, 2011.

[182]. Hendrickson K, Phillips M, Smith W, et al. Hypoxia imaging with [F-18] FMISO-PET in head and neck cancer: potential for guiding intensity modulated radiation therapy in overcoming hypoxia-induced treatment resistance. Radiother Oncol, 2011;101(3):369-75. Epub Aug 27, 2011.

[183]. De Clermont H, Huchet A, Lamare F, Rivière A, Fernandez P. Lack of concordance between the F-18 fluoromisonidazole PET and the F-18 FDG PET in human glioblastoma. Clin Nucl Med, 2011;36(12):e194-5.

[184]. Hugonnet F, Fournier L, Medioni J, et al. Metastatic renal cell carcinoma: relationship between initial metastasis hypoxia, change after 1 month's sunitinib, and therapeutic response: an 18F-fluoromisonidazole PET/CT study. J Nucl Med, 2011;52(7):1048-55. Epub Jun 16, 2011.

[185]. Abolmaali N, Haase R, Koch A, et al. Two or four hour [^{18}F]FMISO-PET in HNSCC. When is the contrast best? Nuklearmedizin, 2011;50(1):22-7. Epub Dec 17, 2010.

[186]. Yamane T, Kikuchi M, Shinohara S, Senda M. Reduction of [(18)F]fluoromisonidazole uptake after neoadjuvant chemotherapy for head and neck squamous cell carcinoma. Mol Imaging Biol, 2011;13(2):227-31.

[187]. Choi W, Lee SW, Park SH, et al. Planning study for available dose of hypoxic tumor volume using fluorine-18-labeled fluoromisonidazole positron emission tomography for treatment of the head and neck cancer. Radiother Oncol, 2010;97(2):176-82. Epub Sep 18, 2010.

[188]. Wang W, Lee NY, Georgi JC, et al. Pharmacokinetic analysis of hypoxia (18)F-fluoromisonidazole dynamic PET in head and neck cancer. J Nucl Med, 2010;51(1):37-45. Epub Dec 15, 2009.

[189]. Szeto MD, Chakraborty G, Hadley J, et al. Quantitive metrics of net proliferation and invasion link biological aggressiveness assessed by MRI with hypoxia assessed by FMISO-PET in newly diagnosed glioblastomas. *Cancer Res*. 2009; 69(10):4502-4509.

[190]. Swanson KR, Chakraborty G, Wang CH, et al. Complementary but distinct roles for MRI and ^{18}F-Fluoromisonidazole PET in the assessment of human glioblastomas. *J Nucl Med*. 2009; 50(1):36-44.

[191]. Lee N, Nehmeh S, Schöder H, et al. Prospective trial incorporating pre-/mid-treatment [^{18}F]-misonidazole positron emission tomography for head-and-neck cancer patients undergoing concurrent chemoradiotherapy. *Int J Radiat Oncol Biol Phys*. 2009; 75(1):101-108.

[192].89. Spence AM, Muzi M, Swanson KR, et al. Regional hypoxia in glioblastoma multiforme quantified with [^{18}F] fluoromisonidazole positron emission tomography before radiotherapy: Correlation time to progression and survival. *Clin Cancer Res*. 2008; 14(9):2623-2630.

[193]. Lin Z, Mechalakos J, Nehmeh S, et al. The influence of changes in tumor hypoxia on dose-painting treatment plans based on ^{18}F-FMISO positron emission tomography. *Int J Radiat Oncol Biol Phys*. 2008; 70(4): 1219-1228.

[194]. Thorwarth D, Alber M. Individualised radiotherapy on the basis of functional imaging with FMISO PET. *Z Med Phys*. 2008; 18:43-50.

[195]. Lee NY, Mechalakos JG, Nehmeh S, et al. Fluorine-18-labeled fluoromisonidazole positron emission and computed tomography-guided intensity-modulated radiotherapy for head and neck cancer: A feasibility study. *Int J Radiat Oncol Biol Phys*. 2008; 70(1),2-13.

[196]. Thorwarth D, Soukup M, Alber M. Dose painting with IMPT, helical tomotherapy and IMXT: A dosimetric comparison. *Radiother Oncol*. 2008; 86:30-34.

[197]. Nehmeh SA, Lee NY, Schröder H, et al. Reproducibility of intratumor distribution of ^{18}F-fluoromisonidazole in head and neck cancer. *Int J Radiat Oncol Biol Phys*. 2008;70(1),:235-242.

[198]. Roels S, Slagmolen P, Nuyts J, et al. Biological image-guided radiotherapy in rectal cancer: Is there a role for FMISO or FLT, next to FDG? *Acta Oncol*. 2008; 47:1237-1248.

[199]. Eschmann SM, Paulsen F, Bedeshem C, et al. Hypoxia-imaging with ^{18}F-misonidazole and PET: Changes of kinetics during radiotherapy of head-and-neck cancer. *Radiother Oncol*. 2007; 83:406-410.

[200]. Spence AM, Muzi M, Link JM, Hoffman JM, Eary JF, Krohn KA. NCI sponsored trial for the evaluation of safety and preliminary efficacy of FLT as a marker of proliferation in patients with recurrent gliomas: Safety studies. *Mol Imaging Biol*. 2008, 10:271-280.

[201]. Gagel B, Piroth M, Pinkawa M, et al. pO polaroghraphy, contrast enhanced color duplex sonography (CDS), [^{18}F] fluoromisonidazole and [^{18}F] fluorodeoxyglucose positron emission tomography: Validated methods for the evaluation of therapy-relevant tumor oxygenation or only bricks in the puzzle of tumor hypoxia? *BMC Cancer*. 2007; 7:113-121.

[202]. Thorwarth D, Eschmann S-M, Paulsen F, Alber M. Hypoxia dose painting by numbers: A planning study. *Int J Radiat Oncol Biol Phys*. 2007; 68(1):291-300.

[203]. Zimny M, Gagel B, DiMartino E, et al. FDG-a marker of tumour hypoxia? A comparison with [^{18}F] fluoromisonidazole and pO_2-polarography in metastatic head and neck cancer. *Eur J Nucl Med Mol Imaging*. 2006 33(12): 1426-1431.

[204]. Cherk MH, Foo SS, Poon AMT, et al. Lack of correlation of hypoxic cell fraction and angiogenesis with glucose metabolic rate in non-small cell lung cancer assessed by ^{18}F-fluoromisonidazoleand ^{18}F-FDG PET. *J Nucl Med*. 2006; 47(12): 1921-1926.

[205]. Rischin D, Hicks RJ, Fisher R, et al. Prognostic significace of [^{18}F]-misonidazole positron emission tomography-detected tumor hypoxia in patients with advanced head and neck cancer randomly assigned to chemoradiation with or without tirapazamine: A substudy of trans-tasman radiation oncology group study 98.02. *J Clin Oncol*. 2006; 24(13): 2098-2104.

[206]. Rajendran JG, Schwartz DL, O'Sullivan J, et al. Tumor hypoxia imaging with [F-18] fluoromisonidazole positron emission tomography in head and neck cancer. *Clin Cancer Res*. 2006; 12(18): 5435-5441.

[207]. Gagel B, Reinartz P, Demirel C, et al. [^{18}F] fluoromisonidazole and [^{18}F] fluorodeoxyglucose positron emission tomography in response evaluation after chemo-/radiotherapy of non-small-cell lung cancer: a feasibility study. *BMC Cancer*. 2006, 6(51): 1-8.

[208]. Cher LM, Murone C, Lawrentschuk N, et al. Correlation of hypoxic cell fraction and angiogenesis with glucose metabolic rate in gliomas using [^{18}F] fluoromisonidazole, ^{18}F-FDG PET, and immunohistochemical studies. *J Nucl Med*. 2006 47(3): 410-418.

[209]. Bruehlmeier M, Roelcke U, Schubiger PA, Ametamey SM. Assessment of hypoxia and perfusion in human brain tumors using PET with ^{18}F-fluoromisonidazole and ^{15}O-H_2O. *J Nucl Med*. 2004; 45(11):1851-1859.

[210]. Gagel B, Reinartz P, DiMartino E, et al. pO_2 polarography versus positron emission tomography ([^{18}F] fluoromisonidazole, [^{18}F]-2-fluoro-2'-deoxyglucose). An appraisal of radiotherapeutically relevant hypoxia. *Strahlenther Onkol*. 2004; 180:616-622.

[211]. Markus R, Reutens DC, Kazui S, et al. Topography and temporal evolution of hypoxic viable tissue identified by ^{18}F-fluoromisonidazole positron emission tomography in humans after ischemic stroke. *Stroke*. 2003; 34:2646-2652.

[212]. Bentzen L, Keiding S, Nordsmark M, et al. Tumour oxygenation assessed by ^{18}F-fluoromisonidazole PET and polarographic needle electrodes in human soft tissue tumours. *Radiother Oncol*. 2003; 67:339-344.

[213]. Rajendran JG, Wilson DC, Conrad EU, et al. [^{18}F]FMISO and [^{18}F]FDG PET imaging in soft tissue sarcomas: correlation of hypoxia, metabolism and VEGF expression. *Eur J Nucl Med Mol Imaging*. 2003; 30(5):695-704.

[214]. Read SJ, Hirano T, Abbott DF, et al. The fate of hypoxic tissue on ^{18}F-fluoromisonidazole positron emission tomography after ischemic stroke. *Ann Neurol*. 2000; 48:228-235.

[215]. Rasey JS, Koh W-J, Evans ML, et al. Quantifying regional hypoxia in human tumors with positron emission tomography of [^{18}F]fluoromisonidazole: a pretherapy study of 37 patients. *Int J Radiat Oncol Biol Phys*. 1996; 36(2):417-428

[216]. Koh W-J, Rasey JS, Evans ML, et al. Imaging of hypoxia in human tumors with [F-18]fluoromisonidazole. *Int J Radiat Oncol Biol Phys*. 1992; 22:199-212

[217]. Lehtiö K, Oikonen V, Grönroos T, et al. Imaging of blood flow and hypoxia in head and neck cancer: Initial evaluation with [^{15}O]H_2O and [^{18}F]Fluoroerythronitroimidazole PET. *J Nucl Med*. 2001; 42:1643-1652

[218]. Yamamoto F, Oka H, Antoku S, Ichiya Y-I, Masuda K, Maeda M. Synthesis and characterization of lipophilic 1-[^{18}F]fluoroalkyl-2- nitroimidazoles for imaging hypoxia. *Biol Pharm Bull.* 1999; 22(6):590-597.

[219]. Sorger D, Patt M, Kumar P, et al. [^{18}F]Fluoroazomycinarabinofuranoside (^{18}FAZA) and [^{18}F]fluoromisonidazole (^{18}FMISO): A comparative study of their selective uptake in hypoxic cells and PET imaging in experimental rat tumors. *Nucl Med Biol*. 2003; 30:317-326.

[220].. Dubois L, Landuyt W, Haustermans K, et al. Evaluation of hypoxia in an experimental rat tumour model by [^{18}F]fluoromisonidazole PET and immunohistochemistry. *Br J Cancer.* 2004; 91:1947-1954.

[221]. Rasey JS, Evans ML. Detecting hypoxia in human tumors. In: Vaupel P, Jain RK, eds. Tumor Blood Supply and Metabolic Microenvironment: Characterizations and Implications for Therapy. Funktionanalyze Biologischer Systeme 20: Gustav Fischer Verlag, New York. 1991; 20:187-201.